PROCEEDINGS A

royalsocietypublishing.org/journal/rspa

Research

Cite this article: Vavryčuk V. 2022 Considering light–matter interactions in the Friedmann equations. *Proc. R. Soc. A* **478**: 20220045.
https://doi.org/10.1098/rspa.2022.0045

Received: 18 January 2022
Accepted: 10 March 2022

Subject Areas:
cosmology

Keywords:
early Universe, cosmic background radiation, dust, extinction, universe opacity, dark energy

Author for correspondence:
V. Vavryčuk
e-mail: vv@ig.cas.cz

Considering light–matter interactions in the Friedmann equations

V. Vavryčuk

Institute of Geophysics, Czech Academy of Sciences, Boční II 1401, Praha 4, 141 00, Czech Republic

VV, 0000-0003-3962-2678

Recent observations indicate that the Universe is not transparent but partially opaque due to absorption of light by ambient cosmic dust. This implies that the Friedmann equations valid for the transparent universe must be modified for the opaque universe. This paper studies a scenario in which the opacity rises with redshift. In this case, the light–matter interactions become important, because cosmic opacity produces radiation pressure that counterbalances gravitational forces. The presented theoretical model assumes the Universe is expanding according to the standard FLRW metric but with the scale factor $a(t)$ depending on both types of forces: gravity as well as radiation pressure. The modified Friedmann equations predict a cyclic expansion/contraction evolution of the Universe within a limited range of scale factors with no initial singularity. The model avoids dark energy and removes some other tensions of the standard cosmological model. The paper demonstrates that considering light–matter interactions in cosmic dynamics is crucial and can lead to new cosmological models essentially different from the standard ΛCDM model. This emphasizes the necessity of new observations and studies of cosmic opacity and cosmic dust at high redshifts for more realistic modelling of the evolution of the Universe.

1. Introduction

Dust is an important component of the interstellar medium (ISM) and intergalactic medium (IGM), which interacts with the stellar radiation. Dust grains absorb

THE ROYAL SOCIETY PUBLISHING

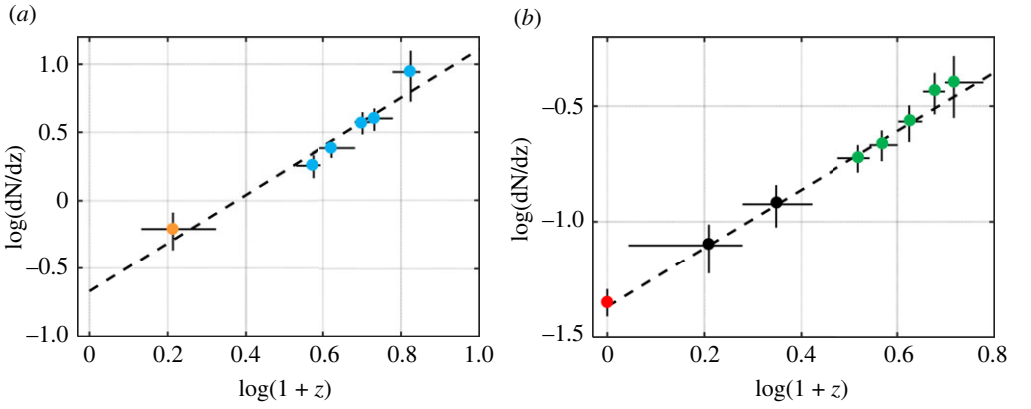

Figure 1. The incidence rate of the LLS (*a*) and DLA systems (*b*) as a function of redshift. The black dashed line—interpolation of observations. The observations are taken from Péroux *et al.* [34]—orange dot, Songaila & Cowie [30]—cyan dots, Zwaan *et al.* [27]—red dot, Rao *et al.* [31]—black dots, and Prochaska and Herbert-Fort [32]—green dots. (Online version in colour.)

and scatter the starlight and reemit the absorbed energy at infrared, far-infrared and microwave wavelengths [1–6]. Since galaxies contain interstellar dust, they lose their transparency and become opaque. The most transparent galaxies are elliptical, while the spiral and irregular galaxies are more opaque, when more than 40% of light of stars in galaxies is absorbed by the galactic dust [7–11]. Similarly, the Universe is not transparent but partially opaque due to ambient cosmic dust. Absorption of light by intergalactic dust grains produces cosmic opacity, which is spatially dependent and varies with frequency and redshift [6,12–15]. It can be measured by dust reddening being particularly appreciable at close distance from galaxies and in intracluster space [16–18]. Ménard *et al.* [18] correlated the brightness of ≈85.000 quasars at $z > 1$ with the position of 24×10^6 galaxies at $z \approx 0.3$ derived from the Sloan Digital Sky Survey, and found an averaged intergalactic attenuation A_V to about 0.03 mag.

Alternatively, the cosmic opacity can be estimated from the hydrogen column densities of Lyman α (Lyα) absorbers. Massive clouds with $N_{\rm HI} \approx 10^{21}\,{\rm cm}^{-2}$, called the damped Ly$\alpha$ absorbers (DLAs), are self-shielded and rich in cosmic dust. They are detected in galaxies as well as in the circumgalactic and intergalactic space [19–23]. Since a relation between the total hydrogen column density $N_{\rm H}$ and the colour excess $E(B-V)$ is known: $N_{\rm H}/E(B-V) = 5.6\text{–}5.8 \times 10^{21}\,{\rm cm}^{-2}\,{\rm mag}^{-1}$ [24,25], we get the ratio $N_{\rm H}/A_V \approx 1.87 \times 10^{21}\,{\rm cm}^{-2}\,{\rm mag}^{-1}$ for $R_V = 3.1$, which is a typical value for our galaxy [1,26]. From observations of the mean cross-section density of DLAs, $\langle n\sigma \rangle = (1.13 \pm 0.15) \times 10^{-5}\,h\,{\rm Mpc}^{-1}$ [27], the characteristic column density of DLAs, $N_{\rm HI} \approx 10^{21}\,{\rm cm}^{-2}$, and the mean molecular hydrogen fraction in DLAs of about 0.4–0.6 [25, their table 8], we obtain the cosmic opacity $\lambda_V \approx 1\text{–}2 \times 10^{-5}\,h\,{\rm Mpc}^{-1}$ at $z = 0$.

The cosmic opacity is very low in the local Universe [16,17], but it might steeply increase with redshift [18,28,29]. Appreciable cosmic opacity at high redshift is documented by observations of (1) the evolution of the Lyα forest of absorption lines in quasar optical spectra, (2) the metallicity detected in the Lyα forest and (3) emission spectra of high-redshift galaxies. In the Lyα forest studies, the evolution of massive Lyman-limit (LLS) and damped Lyman absorption (DLA) systems are, in particular, important, because they serve as reservoirs of dust [19,20]. It has been shown that the incidence rate and the Gunn–Peterson optical depth of the LLS and DLA systems increase with redshift as $(1+z)^4$ or more for $z < 7$ [30–33], see figure 1. For higher z, the increase of the optical depth is even stronger.

Another independent indication of dust at high redshifts is a weak or no evolution of metallicity with redshift. For example, observations of the C_{IV} absorbers do not show any visible redshift evolution over cosmic time suggesting that a large fraction of intergalactic metals may

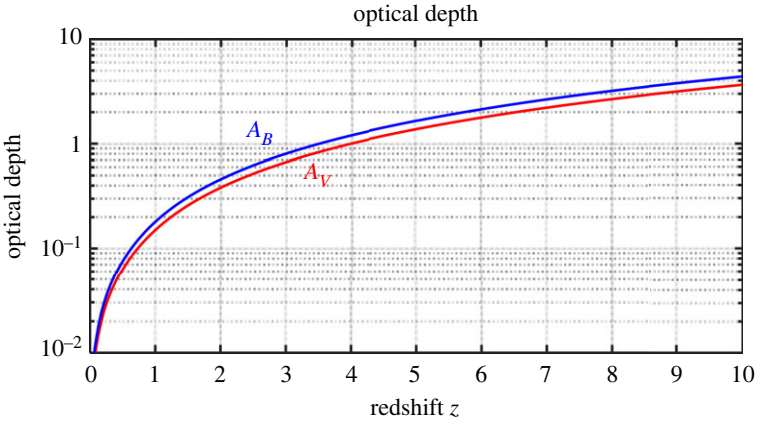

Figure 2. Optical depth of intergalactic space as a function of redshift. The extinction coefficient $R_V = A_V/(E(B-E)$ is assumed to be 5. A_V—extinction at the visual band, A_B—extinction at the B band. For details, see Vavryčuk [6,29]. (Online version in colour.)

already have been in place at $z > 6$ [35–37]. In addition, the presence of dust in the high-redshift universe is documented by observations of dusty galaxies even at $z > 7$ [38,39] and dusty halos around star-forming galaxies at $z = 5$–7 [40]. Zavala *et al.* [41] measured a dust mass of $\approx 10^7 M_\odot$ for a galaxy at $z \approx 9$. Since dust in high-redshift galaxies can efficiently be transported to halos due to galactic wind [12,42] and radiation pressure [43], the cosmic dust must be present even at redshifts $z > 7$–9.

Since dust is traced mostly by reddening of galaxies and quasars at high redshifts, it is difficult to distinguish which portion of reddening is caused by dust present in a galaxy and by cosmic dust along the line of sight. Xie *et al.* [28,44] studied dust extinction using spectra of ≈90.000 quasars from the SDSS DR7 quasar catalogue and tried to separate both the effects. They revealed that quasars have systematically redder UV continuum slopes at higher redshifts and estimated the extinction A_V by cosmic dust of about $\approx 0.02\,\mathrm{Gpc}^{-1}$. This value, however, strongly increases with redshift, because of increase of dust density due to the smaller volume of the Universe in the past [6,29], see figure 2.

The fact that the Universe is not transparent but partially opaque might have fundamental cosmological consequences, because the commonly accepted cosmological model was developed for the transparent universe. Neglecting cosmic opacity produced by intergalactic dust may lead to distorting the observed evolution of the luminosity density and the global stellar mass density with redshift [29]. For example, a decrease of the luminosity density with redshift observed for $z > 2-3$ is commonly explained by darkness of the early Universe. However, this effect can just be an artefact of non-negligible opacity of IGM in the early Universe, when the light coming from high redshifts is attenuated [29]. Figure 3 shows that after eliminating the effect of the opacity from observations, the comoving luminosity density and global stellar mass is redshift independent. Note that physical origin of darkness of the early Universe discussed here is quite different from that of the 'dark ages' in the Big Bang theory. While we study the cosmic opacity due to the presence of dust at redshifts $z < 25$ (dust temperature being less than 80 K), the dark ages epoch is produced by opaque plasma at redshifts $z > 1100$ (plasma temperature being approx. 10^9 K).

Non-zero cosmic opacity may partly or fully invalidate the interpretation of the Type Ia supernova (SNe Ia) dimming as a result of dark energy and the accelerating expansion of the Universe [12,42,61,62]. According to Vavryčuk [13] and Vavryčuk & Kroupa [63], cosmic opacity $\lambda_B \approx 0.08$–$0.10\,\mathrm{Gpc}^{-1}$, which is only 2-3 times higher than its current estimates, fits the Type Ia supernova observations with no need to introduce the accelerated

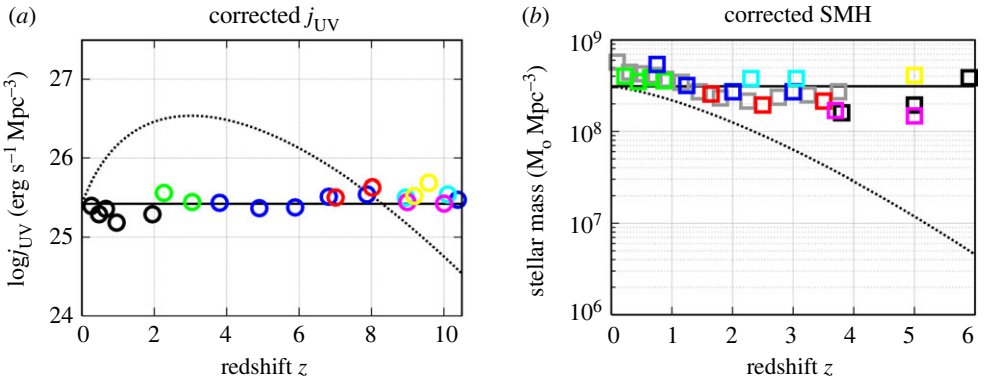

Figure 3. (*a*) The corrected comoving UV luminosity density j_{UV} as a function of redshift after eliminating the effect of the cosmic opacity defined by A_{UV} of 0.08 mag h Gpc^{-1}. Observations are taken from Schiminovich *et al.* [45, black circles], Reddy & Steidel [46, green circles], Bouwens *et al.* [47, blue circles], McLure *et al.* [48, red circles], Ellis *et al.* [49, magenta circles], Oesch *et al.* [50, cyan circles] and Bouwens *et al.* [51, yellow circles]. The dotted line shows the apparent comoving luminosity density, when the bias produced by the cosmic opacity is not eliminated. (*b*) The comoving global stellar mass history (SMH) after eliminating the effect of the cosmic opacity defined by A_{UV} of 0.08 mag h Gpc^{-1}. The colour squares show observations reported by Pérez-González *et al.* [52, grey], Pozzetti *et al.* [53, green], Kajisawa *et al.* [54, blue], Marchesini *et al.* [55, red], Reddy *et al.* [56, cyan], González *et al.* [57, black], Lee *et al.* [58, magenta] and Yabe *et al.* [59, yellow]. The values are summarized in table 2 of Madau & Dickinson [60]. The dotted line shows the apparent comoving SMH, when the bias produced by the cosmic opacity is not eliminated. For details, see Vavryčuk [6]. (Online version in colour.)

expansion. In addition, cosmic dust can produce the cosmic microwave background (CMB) [64–66]. For example, Vavryčuk [6] showed that thermal radiation of dust is capable of explaining the spectrum, intensity and temperature of the CMB including the CMB temperature/polarization anisotropies. In this theory, the CMB temperature fluctuations are caused by fluctuations of the extragalactic background light (EBL) produced by galaxy clusters and voids in the Universe, and the CMB polarization anomalies originate in the polarized thermal emission of needle-shaped conducting dust grains, which are aligned by magnetic fields around large-scale structures such as clusters and voids.

If cosmic opacity and light–matter interactions are considered, the Friedmann equations in the current form are inadequate and must be modified. The radiation pressure, which is caused by absorption of photons by dust grains and acts against gravitational forces, must be incorporated. In this paper, I demonstrate that the radiation pressure due to light absorption is negligible at the present epoch, but it could be significantly stronger in the past epochs. Surprisingly, its rise with redshift could be so steep that it could even balance the gravitational forces at high redshifts and cause the expansion of the Universe. Based on numerical modelling and observations of basic cosmological parameters, I show that the modified Friedmann equations avoid the initial singularity and lead to a cyclic model of the Universe with expansion/contraction epochs within a limited range of scale factors. I estimate the maximum redshift of the Universe achieved in the past and the maximum scale factor of the Universe in the future.

2. Theory

(a) Friedmann equations for the transparent universe

The standard Friedmann equations for the pressureless fluid read [67,68]

$$\left(\frac{\dot{a}}{a}\right)^2 = \frac{8\pi G}{3}\rho - \frac{kc^2}{a^2} + \frac{1}{3}\Lambda c^2 \tag{2.1}$$

royalsocietypublishing.org/journal/rspa Proc. R. Soc. A 478: 20220045

and

$$\frac{\ddot{a}}{a} = -\frac{4\pi G}{3}\rho + \frac{1}{3}\Lambda c^2, \tag{2.2}$$

where $a = (1+z)^{-1}$ is the relative scale factor, G is the gravitational constant, ρ is the mean mass density, k/a^2 is the spatial curvature of the universe, Λ is the cosmological constant and c is the speed of light. Considering mass density ρ as a sum of matter and radiation contributions, we get

$$\frac{8\pi G}{3}\rho = H_0^2[\Omega_m a^{-3} + \Omega_r a^{-4}]. \tag{2.3}$$

Equation (2.1) is then rewritten as

$$H^2(a) = H_0^2[\Omega_m a^{-3} + \Omega_r a^{-4} + \Omega_\Lambda + \Omega_k a^{-2}], \tag{2.4}$$

with the condition

$$\Omega_m + \Omega_r + \Omega_\Lambda + \Omega_k = 1, \tag{2.5}$$

where $H(a) = \dot{a}/a$ is the Hubble parameter, H_0 is the Hubble constant, and Ω_m, Ω_r, Ω_Λ and Ω_k are the normalized matter, radiation, vacuum and curvature terms. Assuming $\Omega_r = 0$ and $\Omega_k = 0$ in equation (2.4), we get the standard ΛCDM model

$$H^2(a) = H_0^2\,[\Omega_m a^{-3} + \Omega_\Lambda], \tag{2.6}$$

which describes a flat, matter-dominated Universe. The Universe is transparent, because any interaction of radiation with matter is neglected. The vacuum term Ω_Λ is called dark energy and it is responsible for the accelerating expansion of the Universe. The dark energy is introduced into equations (2.4)–(2.6) to fit the ΛCDM model with observations of the Type Ia supernova dimming.

(b) Light–matter interaction

The basic drawback of the ΛCDM model is its assumption of transparency of the Universe and the neglect of the Universe opacity caused by interaction of light with intergalactic dust. Absorption of light by cosmic dust produces radiation pressure acting against the gravity, but this pressure is ignored in the ΛCDM model.

Let us consider light emitted by a point source with mass M (in kg) and luminosity L (in W) and absorbed by a dust grain with mass M_D, see figure 4. The light source produces the energy flux I (in W m^{-2}) and the radiation pressure p_D, which acts on the dust grain. The acceleration of the dust grain produced by the light source reads

$$\ddot{R}_\Lambda = \frac{S_D}{M_D} p_D, \tag{2.7}$$

where S_D is the absorption cross-section of the grain. Since the radiation pressure p_D is related to the energy flux I and to the luminosity L as

$$p_D = \frac{I}{c} = \frac{L}{4\pi R^2 c}, \tag{2.8}$$

we get

$$\ddot{R}_\Lambda = \frac{S_D}{M_D}\frac{L}{4\pi c}\frac{1}{R^2}, \tag{2.9}$$

where R is the distance of the dust grain from the light source, and c is the speed of light. The ratio S_D/M_D in equation (2.9) can be expressed as

$$\frac{S_D}{M_D} = \frac{3}{4}\frac{Q_{\mathrm{abs}}}{R_D \rho_D} = \kappa, \tag{2.10}$$

where $S_D = Q_{\mathrm{abs}}\pi R_D^2$ is the absorption cross-section of the dust grain, $M_D = \frac{4}{3}\pi R_D^3 \rho_D$ is the mass of the grain, R_D is the grain radius, Q_{abs} is the grain absorption efficiency, ρ_D is the specific mass

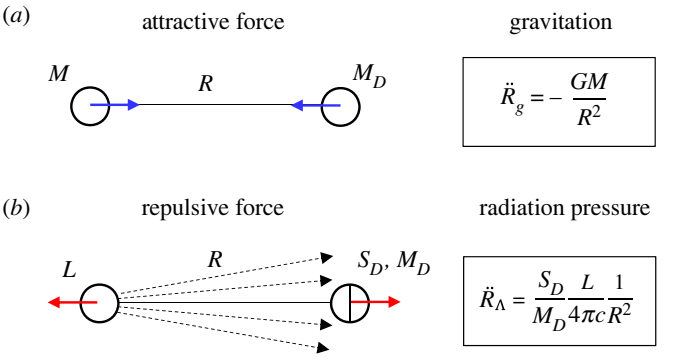

Figure 4. The scheme of gravitational forces (*a*) and radiation pressure (*b*) acting on dust grains. The blue and red arrows indicate a direction of the acting attractive and repulsive forces, respectively. The point source is characterized by mass M and luminosity L. The dust grains have mass M_D and the cross-section S_D. The radiation pressure caused by absorption of energy flux I emitted by the light source with luminosity L decreases with distance as $1/R^2$ similarly as the gravitational force. (Online version in colour.)

density of grains and κ is the mass opacity (in $\mathrm{m^2 kg^{-1}}$). Inserting equation (2.10) into equation (2.9), we write

$$\ddot{R}_\Lambda = \frac{\kappa L}{4\pi c}\frac{1}{R^2}. \tag{2.11}$$

Comparing the radiation–absorption acceleration $\ddot{R}_\Lambda$ with the gravitational acceleration $\ddot{R}_g$

$$\ddot{R}_g = -\frac{GM}{R^2}, \tag{2.12}$$

we see that both accelerations depend on distance from a source in the same way (as $1/R^2$). Consequently, the total acceleration of a dust grain is

$$\ddot{R} = \ddot{R}_g + \ddot{R}_\Lambda = \frac{1}{R^2}\left(-GM + \frac{\kappa L}{4\pi c}\right). \tag{2.13}$$

Dividing equation (2.13) by distance R and substituting mass M (in kg) and luminosity L (in W) by mass density ρ (in $\mathrm{kg\,m^{-3}}$) and luminosity density j (in $\mathrm{W\,m^{-3}}$), we get

$$\frac{\ddot{R}}{R} = -\frac{4\pi G}{3}\rho + \frac{\kappa j}{3c}, \tag{2.14}$$

and consequently, we obtain a generalized Poisson equation for the scalar potential Φ, which involves potentials for both gravitational and radiation–absorption fields

$$\Delta\Phi = 4\pi G\rho - \frac{\kappa j}{c}. \tag{2.15}$$

Equivalently

$$\Delta\Phi = 4\pi G\rho - \rho_\Lambda, \tag{2.16}$$

where $\rho_\Lambda = \kappa j/c$ will be called the density of the radiation–absorption field.

(c) Friedmann equations for the opaque universe

The generalized Poisson equation (2.16) implies that the radiation–absorption term is in many aspects similar to gravity; its effect is, however, opposite. Therefore, deriving the Friedmann equations for the opaque universe using general relativity will be analogous to that for the transparent universe. The only difference is that we have to introduce another term into the Einstein field equations, which will describe a non-gravitational field associated with the light–matter interaction. This term will play the same role as the cosmological constant Λ in equations

(2.1) and (2.2), but in contrast to Λ, which is of unclear physical nature, the light–matter interaction term is physically well justified.

The light–matter interaction will be characterized by density ρ_Λ and pressure p_Λ. The energy-momentum tensor $\Lambda^{\mu\nu}$ of the light–matter interaction will be defined in a similar way as the energy-momentum tensor $T^{\mu\nu}$ for the gravitational field, see appendix A for details. Assuming that the Universe is filled by a perfect homogeneous and isotropic fluid and its expansion is described by the standard FLRW metric, we obtain the following modified Friedmann equations (see equations (A 11) and (A 15) in appendix A):

$$\left(\frac{\dot{a}}{a}\right)^2 = \frac{8\pi G}{3}\rho - \frac{2}{3}\rho_\Lambda - \frac{kc^2}{a^2} \tag{2.17}$$

and

$$\frac{\ddot{a}}{a} = -\frac{4\pi G}{3}(\alpha - 2)\rho + \frac{1}{3}(\beta - 2)\rho_\Lambda, \tag{2.18}$$

where coefficients α and β define the dependence of densities ρ and ρ_Λ on the scale factor $a(t)$: $\rho \sim a^{-\alpha}$ and $\rho_\Lambda \sim a^{-\beta}$. Specifying equation (2.18) for the pressureless fluid ($\alpha = 3$) and taking into account that $\rho_\Lambda = \kappa j/c$, we obtain the final form of the Friedmann equations for the opaque universe

$$\left(\frac{\dot{a}}{a}\right)^2 = \frac{8\pi G}{3}\rho - \frac{2}{3}\frac{\kappa j}{c} - \frac{kc^2}{a^2} \tag{2.19}$$

and

$$\frac{\ddot{a}}{a} = -\frac{4\pi G}{3}\rho + \frac{\beta - 2}{3}\frac{\kappa j}{c}. \tag{2.20}$$

Comparing equations (2.1) and (2.2) with equations (2.19) and (2.20), we see that the modified Friedmann equations can be rewritten into a form almost identical with the original Friedmann equations

$$\left(\frac{\dot{a}}{a}\right)^2 = \frac{8\pi G}{3}\rho - \frac{kc^2}{a^2} + \frac{1}{3}\Lambda c^2 \tag{2.21}$$

and

$$\frac{\ddot{a}}{a} = -\frac{4\pi G}{3}\rho + \frac{2 - \beta}{2}\frac{1}{3}\Lambda c^2, \tag{2.22}$$

if the cosmological term Λ is defined as

$$\Lambda = -2\frac{\kappa j}{c^3}. \tag{2.23}$$

The only difference is in factor $(2 - \beta)/2$ in equation (2.22), originating from the fact that Λ is not a constant any more but depends on the scale factor $a(t)$. If $\beta = 0$, equation (2.22) becomes identical with the Friedmann equation (2.2).

(d) Distance-redshift relation

Assuming that Λ depends on a as $\sim a^{-\beta}$ in equation (2.21), the Hubble parameter reads

$$H^2(a) = H_0^2\left[\Omega_m a^{-3} + \Omega_r a^{-4} + \Omega_a a^{-\beta} + \Omega_k a^{-2}\right], \tag{2.24}$$

where Ω_m, Ω_r, Ω_a and Ω_k are the normalized matter, radiation, radiation–absorption and curvature terms, respectively. In contrast to Ω_m and Ω_r, which describe attractive gravitational forces produced by matter and radiation in the Universe, Ω_a describes repulsive non-gravitational forces produced by the light–matter interaction. Since gravity associated with radiation is non-negligible only for $z > 1100$, we can assume $\Omega_r = 0$ and specify equation (2.24) for the

matter-dominated opaque universe as

$$H^2(a) = H_0^2 \left[\Omega_m a^{-3} + \Omega_a a^{-\beta} + \Omega_k a^{-2}\right], \tag{2.25}$$

with the condition

$$\Omega_m + \Omega_a + \Omega_k = 1, \tag{2.26}$$

where

$$\Omega_m = \frac{1}{H_0^2}\left(\frac{8\pi G}{3}\rho_0\right), \tag{2.27}$$

$$\Omega_a = -\frac{1}{H_0^2}\left(\frac{2}{3}\frac{\kappa_0 j_0}{c}\right), \tag{2.28}$$

and

$$\Omega_k = -\frac{kc^2}{H_0^2}. \tag{2.29}$$

The minus sign in equation (2.28) means that the radiation pressure due to the light–matter interaction acts against the gravity. Considering $a = 1/(1+z)$, the comoving distance is expressed from equation (2.25) as a function of redshift as follows:

$$\mathrm{d}r = \frac{c}{H_0}\frac{\mathrm{d}z}{\sqrt{\Omega_m(1+z)^3 + \Omega_a(1+z)^\beta + \Omega_k(1+z)^2}}. \tag{2.30}$$

(e) Redshift dependence of the light–matter interaction

The radiation–absorption term Λ defined in equation (2.23) is redshift dependent. Under the assumption that the number of sources and their luminosity conserves in time, the rest-frame luminosity density j_ν for a given frequency ν depends on redshift as $(1+z)^3$ and the bolometric luminosity density j depends on redshift as

$$j = j_0 a^{-4} = j_0\,(1+z)^4, \tag{2.31}$$

where subscript '0' corresponds to the quantity observed at present. The assumption of the independence of the global stellar mass in the Universe looks apparently unrealistic but it is fully consistent with observations if corrections to opacity of the high-redshift Universe are applied [6,29], see figure 3.

The luminosity density comprises energy radiated by galaxies into the intergalactic space and thermal radiation of intergalactic dust. All these sources produce cosmic background radiation in the Universe being the sum of the cosmic X-ray background (CXB), the EBL and the cosmic microwave background (CMB). The cosmic background radiation as any radiation in the expanded universe depends on redshift as

$$I = I_0 a^{-4} = I_0\,(1+z)^4. \tag{2.32}$$

Also, the mass opacity κ in equation (2.23) depends on redshift. Based on the extinction law, the mass opacity κ depends on the wavelength λ of absorbed radiation as $\lambda^{-\gamma}$, where γ is the spectral index ranging between 1.0 and 2.0 for grains with size of 0.2 µm or smaller [5,69], see figure 5. Hence, if radiation changes its wavelength due to the redshift, the opacity κ is also redshift dependent. Consequently, the coefficient β describing the redshift-dependent radiation–absorption term in equations (2.25) and (2.30) ranges from 5 to 6. By contrast, the mass opacity is wavelength independent for large grains with size larger than wavelength λ and the radiation–absorption term depends on z as $(1+z)^4$ only.

Since the coefficient β essentially affects the behaviour of the Hubble parameter $H(a)$ and subsequently the evolution of the Universe, we will discuss the origins of its enormously high value in detail. The normalized matter and radiation terms Ω_m and Ω_r in equation (2.24) depend on the scale factor a as a^{-3} and a^{-4}, respectively. Hence, one would intuitively expect that the interaction of matter with radiation will produce term $a^{-\beta}$ with β ranging between 3 and 4.

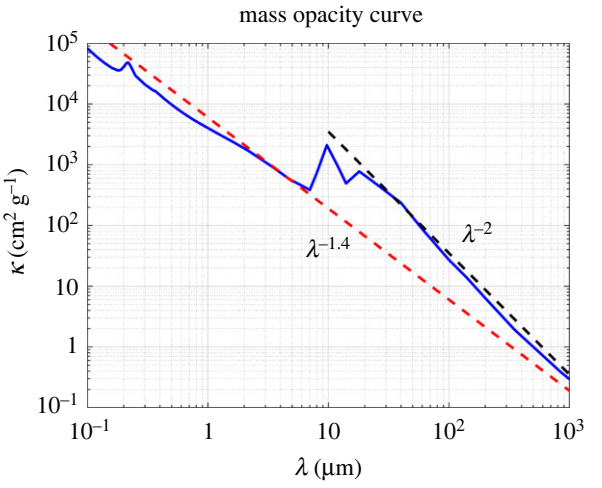

Figure 5. The mass opacity κ as a function of wavelength for the so-called MRN dust model [69] defined by the power-law grains-size distribution with lower and upper size limits between approximately 5 and 250 nm, see tables 4–6 of Draine [4]. The black and red dashed lines show the power law with the spectral index of 2 and 1.4, respectively. (Online version in colour.)

However, this speculation is false, because it ignores the essential property of the radiation-matter interaction—its frequency dependence. The interaction of radiation with matter is caused by absorption of light by grains of cosmic dust, which depends on the wavelength of light and on the size of dust grains. While large wavelengths of light are absorbed weakly, the short wavelengths are absorbed more intensely. Hence, three effects are involved in the light–matter interaction: (1) an increase of the intensity of light as $(1+z)^3$ associated with decreasing the volume of the Universe with redshift, (2) an additional increase of the intensity of light as $(1+z)$ due to the shortening of wavelengths of photons caused by the cosmological redshift and (3) an increase of light absorption as $(1+z)^\gamma$, with γ ranging between 1 and 2, because the photons at high redshifts have shorter wavelengths and interact much more strongly with cosmic dust grains than photons at the present epoch.

(f) Limits of the scale factor a

In order to get simple closed-form formulae, we assume in the next that the mean spectral index γ characterizing the absorption of light by mixture of grains of varying size is 1. Consequently, the radiation–absorption term depends on a as $\sim a^{-5}$. The scale factor a of the Universe with the zero expansion rate is defined by the zero Hubble parameter in equation (2.25), which yields a cubic equation in a

$$\Omega_k a^3 + \Omega_m a^2 + \Omega_a = 0. \tag{2.33}$$

Taking into account that $\Omega_m > 0$ and $\Omega_a < 0$, equation (2.33) has two distinct real positive roots for

$$\left(\frac{\Omega_m}{3}\right)^2 > \left(\frac{\Omega_k}{2}\right)^2 |\Omega_a| \quad \text{and} \quad \Omega_k < 0. \tag{2.34}$$

Negative Ω_a and Ω_k imply that

$$\Omega_m > 1 \quad \text{and} \quad \rho_0 > \rho_c = \frac{8\pi G}{3H_0^2}. \tag{2.35}$$

Under these conditions, equation (2.25) describes a Universe with a cyclic expansion/contraction history and the two real positive roots $a_{\min}$ and $a_{\max}$ define the minimum and maximum scale

factors of the Universe. For $\Omega_a \ll 1$, the scale factors $a_{\min}$ and $a_{\max}$ read approximately

$$a_{\min} \cong \sqrt{\left|\frac{\Omega_a}{\Omega_m}\right|} \quad \text{and} \quad a_{\max} \cong \left|\frac{\Omega_m}{\Omega_k}\right|, \tag{2.36}$$

and the maximum redshift is

$$z_{\max} = \frac{1}{a_{\min}} - 1. \tag{2.37}$$

The scale factors a of the Universe with the maximum expansion/contraction rates are defined by

$$\frac{\mathrm{d}}{\mathrm{d}a} H^2(a) = 0, \tag{2.38}$$

which yields a cubic equation in a

$$2\Omega_k a^3 + 3\Omega_m a^2 + 5\Omega_a = 0. \tag{2.39}$$

Taking into account equations (2.21) and (2.22) and equations (2.27)–(2.29), the deceleration of the expansion reads

$$\ddot{a} = -\frac{1}{2} H_0^2 \left[\Omega_m a^{-2} + 3\Omega_a a^{-4}\right]. \tag{2.40}$$

Hence, the zero deceleration is for the scale factor

$$a = \sqrt{\left|\frac{3\Omega_a}{\Omega_m}\right|}. \tag{2.41}$$

The above equations are quite simple, because they are derived for the spectral index $\gamma = 1$. For other values of γ, the limits of the scale factor a are obtained by solving the equation for the zero Hubble parameter numerically. In general, the higher the spectral index γ, the smaller the value of the maximum redshift $z_{\max}$, see the next sections.

3. Parameters for modelling

To calculate the expansion history and cosmic dynamics of the Universe, we need observations of the mass opacity of intergalactic dust grains, the galaxy luminosity density, the mean mass density, and the expansion rate and curvature of the Universe at the present time.

(a) Mass opacity of cosmic dust

When estimating the mass opacity of dust, κ_0, we have to know the basic parameters of dust grains. The size d of dust grains is in the range of 0.01–0.2 µm with a power-law distribution d^{-q} with $q = 3.5$ [69,70], but silicate and carbonaceous grains dominating the scattering are typically with $d \approx 0.1$ µm [5,71]. The grains of size $0.07\ \mu\mathrm{m} \leq d \leq 0.2\ \mu\mathrm{m}$ are also ejected to the IGM most effectively [72,73]. The grains form complicated fluffy aggregates, which are often elongated or needle-shaped [64,74]. Considering the density of carbonaceous material $\rho \approx 2.2\,\mathrm{g\,cm^{-3}}$ and the silicate density $\rho \approx 3.8\,\mathrm{g\,cm^{-3}}$ [5], the average density of porous dust grains is $\approx 2\,\mathrm{g\,cm^{-3}}$ or less [75–77]. Consequently, the standard dust models [78] predict the wavelength-dependent mass opacity. For example, Draine [4] reports the mass opacity of $855\,\mathrm{m^2\,kg^{-1}}$ at the V-band and the mass opacity of $402\,\mathrm{m^2\,kg^{-1}}$ for a wavelength of 1 µm, which corresponds to the maximum intensity of the EBL.

(b) EBL and the galaxy luminosity density

The EBL covers a wide range of wavelengths from 0.1 to 1000 µm. It was measured, for example, by the IRAS, FIRAS, DIRBE on COBE, and SCUBA instruments; for reviews, see Hauser & Dwek [79], Lagache *et al.* [80], and Cooray [81]. The direct measurements are supplemented by integrating light from extragalactic source counts [79,82] and by attenuation of gamma rays

from distant blazars due to scattering on the EBL [83–86]. The EBL spectrum has two maxima: associated with the radiation of stars (at 0.7–2 μm) and with the thermal radiation of dust in galaxies (at 100–200 μm), see Schlegel *et al.* [2], Calzetti *et al.* [3]. Despite extensive measurements, uncertainties of the EBL are still large. The total EBL should fall between 40 and 200 nW m^{-2} sr^{-1} [6, fig. 1] with the most likely value $I^{\rm EBL} = 80$–$100\,{\rm nW\,m^{-2}\,sr^{-1}}$ [79,87–90].

The galaxy luminosity density is determined from the Schechter function [91]. It has been measured by large surveys 2dFGRS [92], SDSS [93,94] or CS [95]. The luminosity function in the *R*-band was estimated at $z = 0$ to be $(1.84 \pm 0.04) \times 10^8\, h\, L_\odot\, {\rm Mpc}^{-3}$ for the SDSS data [94] and $(1.9 \pm 0.6) \times 10^8\, h\, L_\odot\, {\rm Mpc}^{-3}$ for the CS data [95]. The bolometric luminosity density is estimated by considering the spectral energy distribution (SED) of galaxies averaged over different galaxy types, being thus about 1.7 times larger than that in the *R*-band [29, table 2]: $j_0 \approx 3.1 \times 10^8\, h\, L_\odot\, {\rm Mpc}^{-3}$.

(c) Matter density of the Universe

The simplest and most straightforward method to estimate the matter density is based on galaxy surveys and computation of the mass from the observed galaxy luminosity and from the mass-to-light ratio (M/L) that reflects the total amount of the mass relative to the light within a given scale. The M/L ratio is, however, scale dependent and increases from bright, luminous parts of galaxies to their halos (with radius of ≈200 kpc) formed by (baryonic and/or speculative non-baryonic) dark matter. The M/L ratio depends also on a galaxy type being about three to four times larger for elliptical/SO galaxies than for typical spirals, hence the observed M/L_B is $\approx 100\,h$ for spirals, but $\approx 400\,h$ for ellipticals at radius of ≈200 kpc, see Bahcall *et al.* [96]. Considering the mean asymptotic ratio M/L_B of 200–300 h and the observed mean luminosity density of the Universe at $z = 0$ of $\approx 2.5 \times 10^8\, h\, L_\odot\, {\rm Mpc}^{-3}$ reported by Cross *et al.* [92], the matter density Ω_m associated with galaxies is about 0.2–0.3 ($\Omega_m = 1$ means the critical density).

Another source of matter in the universe is connected to Lyα absorbers containing photoionized hydrogen at $\approx 10^4$ K and being detected by the Lyα forest in quasar spectra [19]. These systems are partly located in the galaxy halos, but a significant portion of them cannot be associated with any galaxy, being observed, for example, in voids [97–99]. The Lyα absorbers also form the intragroup and intracluster medium [100] and the IGM nearby the other large-scale galaxy structures like the galaxy filaments [99,101]. In addition, it is speculated that a large amount of matter is located in the warm-hot intergalactic medium (WHIM) that is a gaseous phase of moderate to low density (≈10–30 times the mean density of the Universe) and at temperatures of 10^5–10^7 K. Although it is difficult to observe the WHIM because of low column densities of HI in the hot gas, they might be potentially detected by surveys of broad HI Lyα absorbers (BLAs) as reported by Nicastro *et al.* [102] or Pessa *et al.* [103].

Hence, we conclude that the estimate of matter density $\Omega_m = 0.2$–0.3 inferred from a distribution of galaxies is just a lower limit, while the upper limit of Ω_m is unconstrained, being possibly close to or even higher than 1. This statement contradicts the commonly accepted value of $\Omega_m = 0.3$ reported by Planck Collaboration *et al.* [104,105] which is based on the interpretation of the CMB as a relic radiation of the Big Bang.

(d) Hubble constant and cosmic curvature

The Hubble constant H_0 is measured by methods based on the Sunyaev-Zel'dovich effect [106–108] or gravitational lensing [109,110], gravitational waves [111–113] or acoustic peaks in the CMB spectrum provided by Planck Collaboration *et al.* [104], and they yield values mostly ranging between 67 and 74 km s^{-1} Mpc^{-1}. Among these approaches, direct methods are considered to be most reliable and accurate (for a review, see Jackson [114]). These methods are based on measuring local distances up to 20–30 Mpc using Cepheid variables observed by the Hubble Space Telescope (HST). The HST galaxies with distance measured with the Cepheid variables are then used to calibrate the SNe Ia data. With this calibration, the distance measure can be extended to other

Table 1. Maximum redshift and scale factor in the cyclic model of the opaque universe. Parameter ε is the ratio of the spheroidal to spherical dust grain cross-sections, Ω_m, Ω_a and Ω_k are the matter, radiation–absorption and curvature terms, β is the power-law exponent describing a decay of the radiation–absorption term with the scale factor a in equation (2.25), and a_{max} and z_{max} are the estimates of the maximum scale factor and redshift, respectively. Models A, B and C predict low, high and optimum values of z_{max}. Models E, D and C predict low, high and optimum values of a_{max}.

	input parameters					output	
model	ε	Ω_m	Ω_a	β	Ω_k	a_{max}	z_{max}
A	6	1.2	-1.7×10^{-3}	5.6	−0.198	6.1	11.4
B	4	1.2	-1.2×10^{-3}	5.2	−0.199	6.0	22.0
C	5	1.2	-1.5×10^{-3}	5.4	−0.199	6.0	15.1
D	5	1.1	-1.5×10^{-3}	5.4	−0.099	11.2	14.6
E	5	1.3	-1.5×10^{-3}	5.4	−0.299	4.4	15.6

more distant galaxies (hundreds of Mpc) in which SNe Ia are detected [115,116]. The estimate of H_0 obtained by Riess *et al.* [117] using the Cepheid calibration is $73.25 \pm 1.74\,\mathrm{km\,s^{-1}\,Mpc^{-1}}$. The precision of the distance scale was further reduced by a factor of 2.5 by Riess *et al.* [118]. Another estimate of H_0 obtained by Freedman *et al.* [119] using the SNe Ia with a red giant branch calibration is $69.8 \pm 2.5\,\mathrm{km\,s^{-1}\,Mpc^{-1}}$.

Assuming the ΛCDM model, the CMB and BAO observations indicate a nearly flat Universe [104]. This method is not, however, model independent and ignores the impact of cosmic dust on the CMB. A model-independent method proposed by Clarkson *et al.* [120] is based on reconstructing the comoving distances by Hubble parameter data and comparing with the luminosity distances [121,122] or the angular diameter distances [123]. The cosmic curvature can also be constrained using strongly gravitational lensed SNe Ia [124] and using lensing time delays and gravitational waves [125]. The authors report the curvature term Ω_k ranging between −0.3 and −0.1 indicating a closed Universe, not significantly departing from flat geometry.

4. Results

Estimating the required cosmological parameters from observations, the upper and lower limits of the volume of the Universe and the evolution of the Hubble parameter with time can be calculated using equations (2.25)–(2.29). The mass density of the Universe higher than the critical density is considered, and subsequently Ω_m is higher than 1. The Hubble constant is $H_0 = 69.8\,\mathrm{km\,s^{-1}\,Mpc^{-1}}$, taken from Freedman *et al.* [119]. The mass opacity κ_0 of $402\,\mathrm{m^2\,kg^{-1}}$ is taken from table 4 of Draine [4] and it characterizes the opacity of dust at a wavelength of 1 µm. The opacity is further multiplied by factor ε reflecting that dust grains are not spherical but rather prolate spheroids having a larger effective cross-section. The luminosity density is $j_0 = 3.1 \times 10^8\, h\, L_\odot\,\mathrm{Mpc^{-3}}$. The radiation–absorption term in equation (2.28) is multiplied by a factor of 2, because photons are not only absorbed but also radiated by dust grains to maintain the thermal equilibrium. The exponent β of the power-law decay of the radiation–absorption term in equation (2.25) ranges from 5.2 to 5.6. The results of modelling are summarized in table 1.

As seen in figure 6, the maximum redshift of the Universe depends on Ω_m and Ω_a, and ranges from 13 to 18 for $\beta = 5.4$. In contrast to a_{min} depending on both Ω_m and Ω_a, the maximum scale factor a_{max} of the Universe depends primarily on Ω_m only. Figure 7 shows that a_{max} rapidly decreases with increasing Ω_m. Obviously, the limiting value is $\Omega_m = 1$, when a_{max} is infinite (flat space). For $\Omega_m = 1.1$, 1.2, 1.3 and 1.5, the scale factor a_{max} is 11.2, 6.0, 4.4 and 3.0, respectively.

The history of the Hubble parameter $H(z)$ and its evolution in the future $H(a)$ calculated by equation (2.25) is shown in figure 8 for five scenarios summarized in table 1. The form of $H(z)$ in figure 8*a* is controlled by Ω_a and the power-law exponent β, while the form of $H(a)$ in figure 8*b*

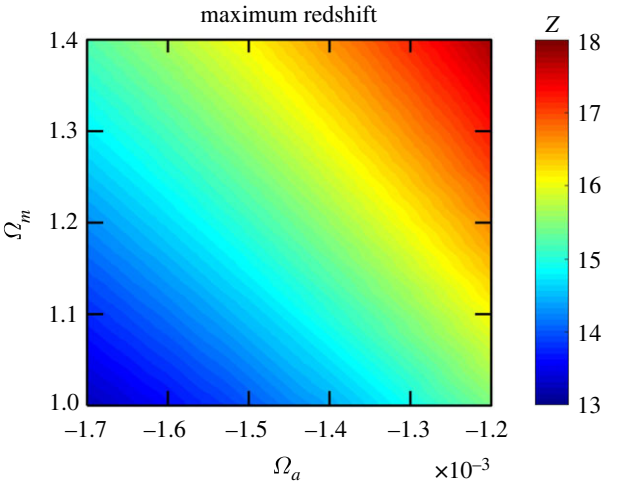

Figure 6. Maximum redshift as a function of Ω_m and Ω_a. The power-law exponent β describing a decay of the radiation–absorption term with the scale factor a is assumed to be 5.4, see table 1. (Online version in colour.)

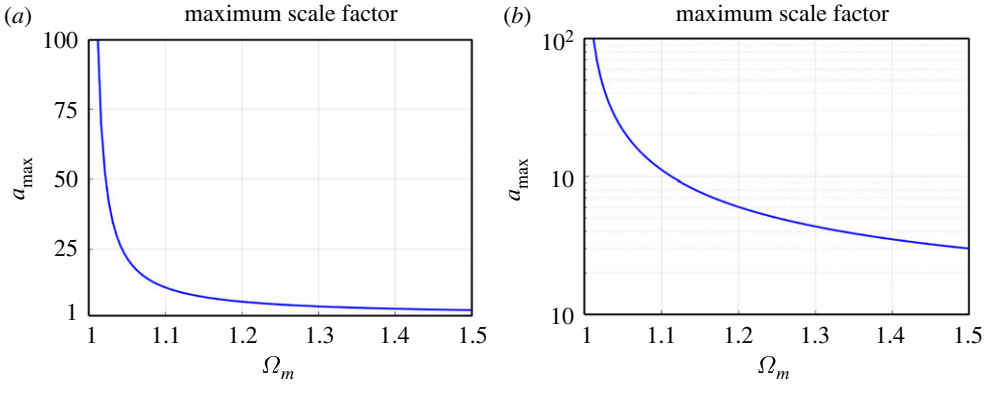

Figure 7. The maximum scale factor as a function of Ω_m. (*a*) Linear scale and (*b*) logarithmic scale. The dependence on Ω_a is negligible. (Online version in colour.)

is controlled by Ω_m. The Hubble parameter $H(z)$ increases with redshift up to its maximum. After that the function rapidly decreases to zero. The drop of $H(z)$ is due to a fast increase of light attenuation producing strong repulsive forces at high redshift. For future epochs, function $H(a)$ is predicted to monotonously decrease to zero. The rate of decrease is controlled just by gravitational forces; the repulsive forces originating in light attenuation are negligible. For a comparison, figure 8 (red line) shows the Hubble parameter $H(a)$ for the standard ΛCDM model [104], which is described by equation (2.6) with $\Omega_m = 0.3$ and $\Omega_\Lambda = 0.7$.

The distance-redshift relation of the proposed cyclic model of the Universe is quite different from the standard ΛCDM model (figure 9). In both models, the comoving distance monotonously increases with redshift, but the redshift can go possibly to 1000 or more in the standard model, while the maximum redshift is likely 14–15 in the optimum cyclic model. The increase of distance with redshift is remarkably steeper for the ΛCDM model than for the cyclic model. The ratio between distances in the cyclic and ΛCDM models rapidly decreases from 1 at $z = 0$ to about 0.63 at $z > 4$.

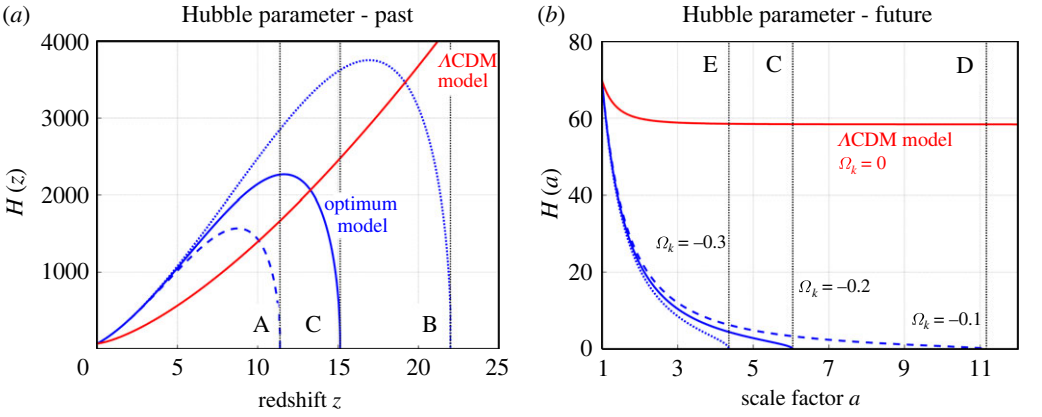

Figure 8. The evolution of the Hubble parameter with redshift in the past and with the scale factor in the future (in km s^{-1} Mpc^{-1}). (*a*) The blue dashed, dotted and solid lines show Models A, B and C in table 1. (*b*) The blue solid, dashed, and dotted lines show Models C, D and E in table 1. The black dotted lines mark the predicted maximum redshifts (*a*) and maximum scale factors (*b*) for the models considered. The red solid line shows the flat ΛCDM model with $H_0 = 69.8$ km s^{-1} Mpc^{-1}, taken from Freedman *et al.* [119], and with $\Omega_m = 0.3$ and $\Omega_\Lambda = 0.7$. (Online version in colour.)

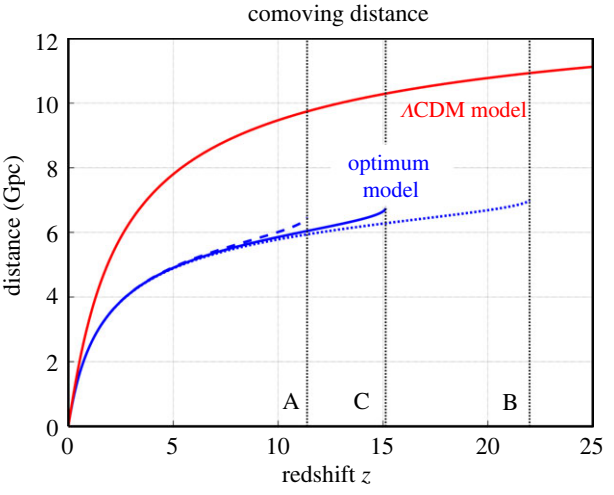

Figure 9. Comoving distance as a function of redshift z. The blue dashed, dotted and solid lines show Models A, B and C in table 1. The black dotted lines mark the predicted maximum redshifts for the models considered. The red solid line shows the flat ΛCDM model with $H_0 = 69.8$ km s^{-1} Mpc^{-1}, taken from Freedman *et al.* [119], and with $\Omega_m = 0.3$ and $\Omega_\Lambda = 0.7$. (Online version in colour.)

5. Other supporting evidence

The cyclic cosmological model of the opaque universe successfully removes some tensions of the standard ΛCDM model:

— The model does not limit the age of stars in the Universe. For example, observations of a nearby star HD 140283 [126] with age of 14.46 ± 0.31 Gyr are in conflict with the age of the Universe, 13.80 ± 0.02 Gyr, determined from the interpretation of the CMB as relic radiation of the Big Bang [104].

— The model predicts the existence of very old mature galaxies at high redshifts. The existence of mature galaxies in the early Universe was confirmed, for example, by Watson *et al.* [38] who analysed observations of the Atacama Large Millimetre Array (ALMA) and revealed a galaxy at $z > 7$ highly evolved with a large stellar mass and heavily enriched in dust. Similarly, Laporte *et al.* [39] analysed a galaxy at $z \approx 8$ with a stellar mass of $\approx 2 \times 10^9 M_\odot$ and a dust mass of $\approx 6 \times 10^6 M_\odot$. A large amount of dust is reported by Venemans *et al.* [127] for a quasar at $z = 7.5$ in the ISM of its host galaxy. In addition, a remarkably bright galaxy at $z \approx 11$ was found by Oesch *et al.* [128] and a significant increase in the number of galaxies for $8.5 < z < 12$ was reported by Ellis *et al.* [49]. Note that the number of papers reporting discoveries of galaxies at $z \approx 10$ or higher is growing rapidly [129–132].

— Assuming 2–3 times higher cosmic opacity than its current estimates, the model is capable of explaining the SNe Ia dimming discovered by Riess *et al.* [133] and Perlmutter *et al.* [134] without introducing dark energy as the hypothetical energy of the vacuum [13], which is difficult to explain under quantum field theory [135]. Moreover, the speed of gravitational waves and the speed of light differ for most dark energy models [136,137], but observations of the binary neutron star merger GW170817 and its electromagnetic counterparts proved that both speeds coincide with a high accuracy.

— The model avoids a puzzle of how the CMB as relic radiation could survive the whole history of the Universe without any distortion [138], and why several unexpected features at large angular scales such as non-Gaussianity [139–141] and a violation of statistical isotropy and scale invariance are observed in the CMB.

— The temperature of the CMB as thermal radiation of cosmic dust is predicted with the accuracy of 2%, see Vavryčuk [6]. The CMB temperature is controlled by the EBL intensity and by the ratio of galactic and intergalactic opacities. The temperature of intergalactic dust increases linearly with redshift and exactly compensates the change of wavelengths due to redshift. Consequently, dust radiation looks apparently like the blackbody radiation with a single temperature.

— The model explains satisfactorily: (1) the observed bolometric intensity of the EBL with a value of $\approx 100\,\mathrm{nW\,m^{-1}\,sr^{-1}}$, see Vavryčuk [29], (2) the redshift evolution of the comoving UV luminosity density with extremely high values at redshifts $2 < z < 4$, see Vavryčuk [6] (fig. 11), and (3) a strong decay of the global stellar mass density at high redshifts, see Vavryčuk [6] (fig. 12). The increase of the luminosity density at $z \approx 2$–3 does not originate in the evolution of the star formation rate as commonly assumed but in the change of the proper volume of the Universe. The decrease of the luminosity density at high z originates in the opacity of the high-redshift universe.

Note that the prediction of a close connection between the CMB anisotropies and the large-scale structures is common to both the standard model and the opaque universe model. The arguments are, however, reversed. The Big Bang theory assumes that the large-scale structures are a consequence of the CMB fluctuations originating at redshifts $z \approx 1100$, while the opaque universe model considers the CMB fluctuations as a consequence of the large-scale structures at redshifts less than 3–5. The polarization anomalies of the CMB correlated with temperature anisotropies are caused by the polarized thermal emission of needle-shaped conducting dust grains aligned by large-scale magnetic fields around clusters and voids. The phenomenon is analogous to the polarized interstellar dust emission in our Galaxy, which is observed at shorter wavelengths because the temperature of the galactic dust is higher than that of the intergalactic dust [142–146].

6. Discussion

The standard Friedmann equations were derived for the transparent universe and assume no light–matter interaction. The equations contain densities Ω_m and Ω_r that describe the effects

of gravity produced by matter, radiation and radiation pressure of photon gas. Since radiation pressure represents energy, it produces also gravity according to general relativity. The effects of radiation are, however, significant only for $z > 1100$. The modified Friedmann equations contain another density Ω_a, which is also connected with the radiation pressure but in a different way. This pressure is produced by absorption of photons by ambient cosmic dust and it acts against gravity.

The radiation pressure as a cosmological force acting against the gravity has not been proposed yet, even though its role is well known in the stellar dynamics [147]. The radiation pressure is important in the evolution of massive stars [148], in supernovae stellar winds and in galactic wind dynamics [42,43,149,150]. Apparently, the radiation pressure in the evolution of the Universe was overlooked, because the Universe was assumed to be transparent. By contrast, the role of radiation pressure is essential in the opaque universe model, because it is produced by absorption of photons by cosmic dust. Since the cosmic opacity and the intensity of the EBL steeply rise with redshift (figure 2), the radiation pressure, negligible at present, becomes significant at high redshifts and can fully eliminate gravity and stop the Universe contraction. In this process, small dust grains will probably be more important, because the mass opacity responsible for the radiation pressure rapidly increases with decreasing size of grains. Similarly, the emission of high-energy photons will affect the Universe dynamics more distinctly than the photons re-emitted by dust grains which form the CMB. The high-energy photons emitted by stars are absorbed by three to four orders more efficiently compared to the CMB photons, which are absorbed by dust very weakly.

Hence, the expansion/contraction evolution of the Universe might be a result of imbalance of gravitational forces and radiation pressure. Since the comoving global stellar and dust masses are basically independent of time with minor fluctuations only (figure 3), the evolution of the Universe is stationary. The age of the Universe in the cyclic model is unconstrained and galaxies can be observed at any redshift less than the maximum redshift $z_{\max}$. The only limitation is high cosmic opacity, which can prevent observations of the most distant galaxies. Hypothetically, it is possible to observe galaxies from the previous cycle/cycles, if their distance is higher than that corresponding to $z_{\max} \approx 14$–15. The identification of galaxies from the previous cycles will be, however, difficult, because their redshift will be a periodic function with increasing distance.

Obviously, a role of recycling processes is much more important in the cyclic cosmological model than in the Big Bang theory. The processes of formation/destruction of galaxies and their interaction with the circumgalactic medium through galactic winds and outflows [151–156] should play a central role in this model. Similarly, the formation of metals in nuclear fusion should be balanced in the long term by their destruction invoked, for example, by quasars. Indications supporting that such a scenario is not ruled out are provided by studies of metallicity with cosmic time, when observations do not show convincing evidence of the metallicity evolution. By contrast, they indicate [19,157,158] a widespread metal pollution of the IGM in all epochs of the Universe and a failure to detect a pristine material with no metals at high redshifts.

In summary, the opaque universe model and the Big Bang theory are completely different concepts of the Universe. Both theories successfully predict basic astronomical observations such as the Universe expansion, the luminosity density evolution with redshift, the global stellar mass history, the SNe Ia measurements and the CMB observations. However, the Big Bang theory needs the existence of dark matter and dark energy, which are supported by no firm evidence. Moreover, they contradict small-scale observations in galaxies [159–162] and are disfavoured by observations of gravitational waves [137]. By contrast, the model of the eternal cyclic universe with high-redshift opacity is based on the standard physics, it is less speculative and predicts the current observations comparably well with no free parameters such as dark energy or dark matter. Nevertheless, this model opens other fundamental questions, such as about recycling processes of stars, galaxies and other objects in the Universe or about similarity/dissimilarity of individual cycles.

Data accessibility. This article has no additional data.

Conflict of interest declaration. I declare I have no competing interests.
Funding. The author received funding from the Institute of Geophysics, Czech Academy of Sciences.
Acknowledgements. I am very thankful for constructive and fruitful comments and suggestions of the Editor and three anonymous referees.

Appendix A. Considering light–matter interactions in Einstein equations of general relativity

The Einstein field equations read

$$G^{\mu\nu} + \Lambda g^{\mu\nu} = \frac{8\pi G}{c^4} T^{\mu\nu}, \tag{A 1}$$

where $G^{\mu\nu}$ is the Einstein tensor, Λ is the cosmological constant, $g^{\mu\nu}$ is the metric tensor, G is the gravitational constant, c is the speed of light and $T^{\mu\nu}$ is the energy-momentum tensor. The Einstein tensor $G^{\mu\nu}$ describes the curvature of the space–time associated with gravity produced by the presence of matter and/or energy described by the energy-momentum tensor $T^{\mu\nu}$.

Since $G^{\mu\nu}{}_{;\nu} = 0$ and $g^{\mu\nu}{}_{;\nu} = 0$, we get

$$T^{\mu\nu}{}_{;\nu} = 0, \tag{A 2}$$

which expresses the energy-momentum conservation law.

The cosmological constant Λ in equation (A 1) represents a non-gravitational field acting against the gravity. It was inserted into the equations by Einstein [163] in order to maintain the Universe as static. Since the physical nature of Λ was unclear, Einstein assumed the cosmological term in the simplest possible form. However, other forms of the cosmological term are, in principle, admissible. Obviously, the validity of the field equations (A 1) is kept, if the cosmological term $\Lambda g^{\mu\nu}$ is substituted by the following more general term $\psi \Lambda^{\mu\nu}$,

$$G^{\mu\nu} + \psi \Lambda^{\mu\nu} = \frac{8\pi G}{c^4} T^{\mu\nu}, \tag{A 3}$$

where ψ is a constant, which should be determined, and $\Lambda^{\mu\nu}$ is the energy-momentum tensor of a non-gravitational field obeying the energy-momentum conservation law

$$\Lambda^{\mu\nu}{}_{;\nu} = 0. \tag{A 4}$$

In the next, tensor $\Lambda^{\mu\nu}$ in equation (A 3) will be interpreted as the result of the light–matter interaction described in section 2(b) Light–matter interaction. The constant ψ standing at $\Lambda^{\mu\nu}$ in equation (A 3) will be determined by applying the weak-field non-relativistic approximation, similarly as for determining the constant $8\pi G/c^4$ standing at the energy-momentum tensor $T^{\mu\nu}$.

Note that tensor $\Lambda^{\mu\nu}$ can formally be a part of the energy-momentum tensor $T^{\mu\nu}$. However, it is useful to treat it separately, in order to emphasize its non-gravitational nature similarly as done by Einstein in the case of the original cosmological constant Λ. In this way, tensor $T^{\mu\nu}$ is allocated for gravitational effects of mass and other physical fields only, but it does not reflect non-gravitational forces. Obviously, both approaches are mathematically equivalent, because if $\Lambda^{\mu\nu}$ is considered as a part of $T^{\mu\nu}$, matching the field equations for a weak non-relativistic field leads finally to decoupling of $\Lambda^{\mu\nu}$ and cancelling the factor $8\pi G/c^4$ standing at the term with $\Lambda^{\mu\nu}$.

For a perfect isotropic fluid, the energy-momentum tensor $T^{\mu\nu}$ reads

$$T^{\mu\nu} = \left(\rho + \frac{p}{c^2}\right) U^\mu U^\nu + p g^{\mu\nu}, \tag{A 5}$$

where ρ is the density, p is the pressure and U^μ is the four velocity. In analogy to (A 5), the isotropic cosmological tensor $\Lambda^{\mu\nu}$ can be described as

$$\Lambda^{\mu\nu} = \left(\rho_\Lambda + \frac{p_\Lambda}{c^2}\right) U^\mu U^\nu + p_\Lambda g^{\mu\nu}, \tag{A 6}$$

where ρ_Λ is the density, and p_Λ is the pressure of the non-gravitational field produced by the light–matter interaction.

The unknown constant ψ in equation (A 3) can now be found in a straightforward way assuming the weak-field approximation and using equation (2.16). This equation can be split into the Poisson equations for the gravitational potential Φ_G and for the potential of the light–matter interaction Φ_Λ as follows:

$$\Delta\Phi_G = 4\pi G\rho \tag{A 7}$$

and

$$\Delta\Phi_\Lambda = -\rho_\Lambda. \tag{A 8}$$

Taking into account that $\Lambda^{00} = \rho_\Lambda c^2$ and applying exactly the same procedure as when determining the constant $8\pi G/c^4$ standing at tensor $T^{\mu\nu}$ in equation (A 1), we get $\psi = 2/c^4$. Hence, equation (A 3) finally reads

$$G^{\mu\nu} + \frac{2}{c^4}\Lambda^{\mu\nu} = \frac{8\pi G}{c^4}T^{\mu\nu}. \tag{A 9}$$

Introducing the standard FLRW metric of the space defined by its Gaussian curvature k and by the scale factor $a(t)$ [67,68]

$$-c^2\,\mathrm{d}\tau^2 = -c^2\,\mathrm{d}t^2 + a^2(t)\left(\frac{\mathrm{d}r^2}{1-kr^2} + r^2\,\mathrm{d}\Omega^2\right), \tag{A 10}$$

in equations (A 9), (A 5) and (A 6), we get a modified form of the Friedmann equations, which involve effects of the non-gravitational field $\Lambda^{\mu\nu}$

$$\left(\frac{\dot{a}}{a}\right)^2 = \frac{8\pi G}{3}\rho - \frac{2}{3}\rho_\Lambda - \frac{kc^2}{a^2} \tag{A 11}$$

and

$$\frac{\ddot{a}}{a} = -\frac{4\pi G}{3}\left(\rho + \frac{3p}{c^2}\right) + \frac{1}{3}\left(\rho_\Lambda + \frac{3p_\Lambda}{c^2}\right). \tag{A 12}$$

Considering ρ and ρ_Λ depending on the scale factor $a(t)$ as $\rho = \rho_0 a^{-\alpha}$ and $\rho_\Lambda = \rho_{\Lambda 0} a^{-\beta}$, the equations of state for $T^{\mu\nu}$ and $\Lambda^{\mu\nu}$ yield

$$p = \frac{\alpha - 3}{3}c^2\rho \tag{A 13}$$

and

$$p_\Lambda = \frac{\beta - 3}{3}c^2\rho_\Lambda, \tag{A 14}$$

and equation (A 12) reads

$$\frac{\ddot{a}}{a} = -\frac{4\pi G}{3}(\alpha - 2)\rho + \frac{1}{3}(\beta - 2)\rho_\Lambda. \tag{A 15}$$

References

1. Mathis JS. 1990 Interstellar dust and extinction. *Annu. Rev. Astron. Astrophys.* **28**, 37–70. (doi:10.1146/annurev.aa.28.090190.000345)
2. Schlegel DJ, Finkbeiner DP, Davis M. 1998 Maps of dust infrared emission for use in estimation of reddening and cosmic microwave background radiation foregrounds. *Astrophys. J.* **500**, 525–553. (doi:10.1086/305772)
3. Calzetti D, Armus L, Bohlin RC, Kinney AL, Koornneef J, Storchi-Bergmann T. 2000 The dust content and opacity of actively star-forming galaxies. *Astrophys. J.* **533**, 682–695. (doi:10.1086/308692)
4. Draine BT. 2003 Interstellar dust grains. *Annu. Rev. Astron. Astrophys.* **41**, 241–289. (doi:10.1146/annurev.astro.41.011802.094840)
5. Draine BT. 2011 *Physics of the interstellar and intergalactic medium*. Princeton, NJ: Princeton University Press.

6. Vavryčuk V. 2018 Universe opacity and CMB. *Mon. Not. R. Astron. Soc.* **478**, 283–301. (doi:10.1093/mnras/sty974)
7. Calzetti D. 2001 The dust opacity of star-forming galaxies. *Publ. Astron. Soc. Pac.* **113**, 1449. (doi:10.1086/324269)
8. Holwerda BW, Gonzalez RA, Allen RJ, van der Kruit PC. 2005 The opacity of spiral galaxy disks. III. Automating the synthetic field method. *Astron. J.* **129**, 1381–1395. (doi:10.1086/427711)
9. Holwerda BW, Draine B, Gordon KD, González RA, Calzetti D, Thornley M, Buckalew B, Allen RJ, van der Kruit PC. 2007 The opacity of spiral galaxy disks. VIII. Structure of the cold ISM. *Astron. J.* **134**, 2226–2235. (doi:10.1086/522230)
10. Finkelman I *et al.* 2008 Determining the extragalactic extinction law with SALT∗. *Mon. Not. R. Astron. Soc.* **390**, 969–984. (doi:10.1111/j.1365-2966.2008.13785.x)
11. Lisenfeld U, Relaño M, Vílchez J, Battaner E, Hermelo I. 2008 Low-metallicity star formation: from the first stars to dwarf galaxies. In *IAU Symposium, vol. 255* (eds LK Hunt, SC Madden, R Schneider), pp. 260–264. Cambridge, UK: Cambridge University Press. (doi:10.1017/S1743921308024915)
12. Aguirre A. 1999 Intergalactic dust and observations of Type Ia supernovae. *Astrophys. J.* **525**, 583–593. (doi:10.1086/307945)
13. Vavryčuk V. 2019 Universe opacity and Type Ia supernova dimming. *Mon. Not. R. Astron. Soc.* **489**, L63–L68. (doi:10.1093/mnrasl/slz128)
14. Aguirre AN. 2000 The cosmic background radiation in a cold big bang. *Astrophys. J.* **533**, 1–18. (doi:10.1086/308660)
15. Corasaniti PS. 2006 The impact of cosmic dust on supernova cosmology. *Mon. Not. R. Astron. Soc.* **372**, 191–198. (doi:10.1111/j.1365-2966.2006.10825.x)
16. Chelouche D, Koester BP, Bowen DV. 2007 The dust content of galaxy clusters. *Astrophys. J. Lett.* **671**, L97–L100. (doi:10.1086/525251)
17. Muller S, Wu S-Y, Hsieh B-C, González RA, Loinard L, Yee HKC, Gladders MD. 2008 Searching for dust in the intracluster medium from reddening of background galaxies. *Astrophys. J.* **680**, 975–980. (doi:10.1086/529583)
18. Ménard B, Scranton R, Fukugita M, Richards G. 2010 Measuring the galaxy–mass and galaxy–dust correlations through magnification and reddening. *Mon. Not. R. Astron. Soc.* **405**, 1025–1039. (doi:10.1111/j.1365-2966.2010.16486.x)
19. Meiksin AA. 2009 The physics of the intergalactic medium. *Rev. Mod. Phys.* **81**, 1405–1469. (doi:10.1103/RevModPhys.81.1405)
20. Wolfe AM, Gawiser E, Prochaska JX. 2005 Damped Lyα systems. *Annu. Rev. Astron. Astrophys.* **43**, 861–918. (doi:10.1146/annurev.astro.42.053102.133950)
21. Ménard B, Fukugita M. 2012 Cosmic dust in Mg II absorbers. *Astrophys. J.* **754**, 116. (doi:10.1088/0004-637X/754/2/116)
22. Peek JEG, Ménard B, Corrales L. 2015 Dust in the circumgalactic medium of low-redshift galaxies. *Astrophys. J.* **813**, 7. (doi:10.1088/0004-637X/813/1/7)
23. Tumlinson J, Peeples MS, Werk JK. 2017 The circumgalactic medium. *Annu. Rev. Astron. Astrophys.* **55**, 389–432. (doi:10.1146/annurev-astro-091916-055240)
24. Bohlin RC, Savage BD, Drake JF. 1978 A survey of interstellar HI from L-alpha absorption measurements. II. *Astrophys. J.* **224**, 132–142. (doi:10.1086/156357)
25. Rachford BL *et al.* 2002 A *Far Ultraviolet Spectroscopic Explorer* survey of interstellar molecular hydrogen in translucent clouds. *Astrophys. J.* **577**, 221–244. (doi:10.1086/342146)
26. Cardelli JA, Clayton GC, Mathis JS. 1989 The relationship between infrared, optical, and ultraviolet extinction. *Astrophys. J.* **345**, 245. (doi:10.1086/167900)
27. Zwaan MA, van der Hulst JM, Briggs FH, Verheijen MAW, Ryan-Weber EV. 2005 Reconciling the local galaxy population with damped Lyman α cross-sections and metal abundances. *Mon. Not. R. Astron. Soc.* **364**, 1467–1487. (doi:10.1111/j.1365-2966.2005.09698.x)
28. Xie X, Shen S, Shao Z, Yin J. 2015 An apparent redshift dependence of quasar continuum: implication for cosmic dust extinction? *Astrophys. J. Lett.* **802**, L16. (doi:10.1088/2041-8205/802/2/L16)
29. Vavryčuk V. 2017 Universe opacity and EBL. *Mon. Not. R. Astron. Soc.* **465**, 1532–1542. (doi:10.1093/mnras/stw2825)
30. Songaila A, Cowie LL. 2010 The evolution of Lyman limit absorption systems to redshift six. *Astrophys. J.* **721**, 1448–1466. (doi:10.1088/0004-637X/721/2/1448)

31. Rao SM, Turnshek DA, Nestor DB. 2006 Damped Lyα Systems at $Z < 1.65$: the expanded sloan digital sky survey *Hubble Space Telescope* sample. *Astrophys. J.* **636**, 610–630. (doi:10.1086/498132)
32. Prochaska JX, Herbert-Fort S. 2004 The SDSS damped Lya survey: data release 1. *Publ. Astron. Soc. Pac.* **116**, 622. (doi:10.1086/421985)
33. Fan X *et al.* 2006 Constraining the evolution of the ionizing background and the epoch of reionization with $z \sim 6$ quasars. II. A sample of 19 quasars. *Astron. J.* **132**, 117–136. (doi:10.1086/504836)
34. Péroux C, McMahon RG, Storrie-Lombardi LJ, Irwin MJ. 2003 The evolution of $\Omega_{\rm HI}$ and the epoch of formation of damped Lyman α absorbers. *Mon. Not. R. Astron. Soc.* **346**, 1103–1115. (doi:10.1111/j.1365-2966.2003.07129.x)
35. Songaila A. 2001 The minimum universal metal density between redshifts of 1.5 and 5.5. *Astrophys. J. Lett.* **561**, L153–L156. (doi:10.1086/324761)
36. Pettini M, Madau P, Bolte M, Prochaska JX, Ellison SL, Fan X. 2003 The C_{IV} mass density of the universe at redshift 5∗. *Astrophys. J.* **594**, 695–703. (doi:10.1086/377043)
37. Ryan-Weber EV, Pettini M, Madau P. 2006 Intergalactic C_{IV} absorption at redshifts 5.4 to 6. *Mon. Not. R. Astron. Soc.* **371**, L78–L82. (doi:10.1111/j.1745-3933.2006.00212.x)
38. Watson D, Christensen L, Knudsen KK, Richard J, Gallazzi A, Michałowski MJ. 2015 A dusty, normal galaxy in the epoch of reionization. *Nature* **519**, 327–330. (doi:10.1038/nature14164)
39. Laporte N, Ellis RS, Boone F, Bauer FE, Quénard D, Roberts-Borsani GW, Pelló R, Pérez-Fournon I, Streblyanska A. 2017 Dust in the reionization era: ALMA observations of a $z = 8.38$ gravitationally lensed galaxy. *Astrophys. J. Lett.* **837**, L21. (doi:10.3847/2041-8213/aa62aa)
40. Fujimoto S *et al.* 2019 First identification of 10 kpc $[C_{II}]$ 158 μm halos around star-forming galaxies at $z = 5$–7. *Astrophys. J.* **887**, 107. (doi:10.3847/1538-4357/ab480f)
41. Zavala JA *et al.* 2015 Early science with the large millimeter telescope: dust constraints in a $z \sim 9.6$ galaxy. *Mon. Not. R. Astron. Soc.* **453**, L88–L92. (doi:10.1093/mnrasl/slv100)
42. Aguirre AN. 1999 Dust versus cosmic acceleration. *Astrophys. J.* **512**, L19–L22. (doi:10.1086/311862)
43. Hirashita H, Inoue AK. 2019 Radiation-pressure-driven dust transport to galaxy haloes at $z \sim 10$. *Mon. Not. R. Astron. Soc.* **487**, 961–974. (doi:10.1093/mnras/stz1348)
44. Xie X, Shao Z, Shen S, Liu H, Li L. 2016 The luminosity dependence of quasar UV continuum slope: dust extinction scenario. *Astrophys. J.* **824**, 38. (doi:10.3847/0004-637X/824/1/38)
45. Schiminovich D *et al.* 2005 The *GALEX*-VVDS measurement of the evolution of the far-ultraviolet luminosity density and the cosmic star formation rate. *Astrophys. J. Lett.* **619**, L47–L50. (doi:10.1086/427077)
46. Reddy NA, Steidel CC. 2009 A steep faint-end slope of the uv luminosity function at $z \sim$ 2–3: implications for the global stellar mass density and star formation in low-mass halos. *Astrophys. J.* **692**, 778–803. (doi:10.1088/0004-637X/692/1/778)
47. Bouwens RJ *et al.* 2014 UV-continuum slopes of > 4000 $z \sim 4$–8 galaxies from the HUDF/XDF, HUDF09, ERS, CANDELS-South, and CANDELS-North fields. *Astrophys. J.* **793**, 115. (doi:10.1088/0004-637X/793/2/115)
48. McLure RJ *et al.* 2013 A new multifield determination of the galaxy luminosity function at $z = 7$–9 incorporating the 2012 Hubble Ultra-Deep Field imaging. *Mon. Not. R. Astron. Soc.* **432**, 2696–2716. (doi:10.1093/mnras/stt627)
49. Ellis RS *et al.* 2013 The abundance of star-forming galaxies in the redshift range 8.5–12: new results from the 2012 Hubble ultra deep field campaign. *Astrophys. J. Lett.* **763**, L7. (doi:10.1088/2041-8205/763/1/L7)
50. Oesch PA *et al.* 2014 The most luminous $z \sim 9$–10 galaxy candidates yet found: the luminosity function, cosmic star-formation rate, and the first mass density estimate at 500 Myr. *Astrophys. J.* **786**, 108. (doi:10.1088/0004-637X/786/2/108)
51. Bouwens RJ *et al.* 2014 A census of star-forming galaxies in the $Z \sim 9$–10 universe based on HST + SPITZER observations over 19 clash clusters: three candidate $Z \sim 9$–10 galaxies and improved constraints on the star formation rate density at $Z \sim 9.2$. *Astrophys. J.* **795**, 126. (doi:10.1088/0004-637X/795/2/126)
52. Pérez-González PG *et al.* 2008 The stellar mass assembly of galaxies from $z = 0$ to $z = 4$: analysis of a sample selected in the rest–frame near–infrared with *spitzer*. *Astrophys. J.* **675**, 234–261. (doi:10.1086/523690)

53. Pozzetti L *et al.* 2010 zCOSMOS–10k-bright spectroscopic sample-the bimodality in the galaxy stellar mass function: exploring its evolution with redshift. *Astron. Astrophys.* **523**, A13. (doi:10.1051/0004-6361/200913020)
54. Kajisawa M *et al.* 2009 Moircs deep survey. IV. Evolution of galaxy stellar mass function back to $z \sim 3$. *Astrophys. J.* **702**, 1393–1412. (doi:10.1088/0004-637X/702/2/1393)
55. Marchesini D, van Dokkum PG, Förster Schreiber NM, Franx M, Labbé I, Wuyts S. 2009 The evolution of the stellar mass function of galaxies from $z = 4.0$ and the first comprehensive analysis of its uncertainties: evidence for mass-dependent evolution. *Astrophys. J.* **701**, 1765–1796. (doi:10.1088/0004-637X/701/2/1765)
56. Reddy N *et al.* 2012 Goods-Herschel measurements of the dust attenuation of typical star-forming galaxies at high redshift: observations of ultraviolet-selected galaxies at $z \sim 2$. *Astrophys. J.* **744**, 154. (doi:10.1088/0004-637X/744/2/154)
57. González V, Labbé I, Bouwens RJ, Illingworth G, Franx M, Kriek M. 2011 Evolution of galaxy stellar mass functions, mass densities, and mass-to-light ratios from $z \sim 7$ to $z \sim 4$. *Astrophys. J. Lett.* **735**, L34. (doi:10.1088/2041-8205/735/2/L34)
58. Lee K-S *et al.* 2012 How do star-forming galaxies at $z > 3$ assemble their masses? *Astrophys. J.* **752**, 66. (doi:10.1088/0004-637X/752/1/66)
59. Yabe K, Ohta K, Iwata I, Sawicki M, Tamura N, Akiyama M, Aoki K. 2009 The stellar populations of Lyman break galaxies at $z \sim 5$. *Astrophys. J.* **693**, 507–533. (doi:10.1088/0004-637X/693/1/507)
60. Madau P, Dickinson M. 2014 Cosmic star-formation history. *Annu. Rev. Astron. Astrophys.* **52**, 415–486. (doi:10.1146/annurev-astro-081811-125615)
61. Aguirre A, Haiman Z. 2000 Cosmological constant or intergalactic dust? Constraints from the cosmic far-infrared background. *Astrophys. J.* **532**, 28–36. (doi:10.1086/308557)
62. Ménard B, Kilbinger M, Scranton R. 2010 On the impact of intergalactic dust on cosmology with Type Ia supernovae. *Mon. Not. R. Astron. Soc.* **406**, 1815–1820. (doi:10.1111/j.1365-2966.2010.16464.x)
63. Vavryčuk V, Kroupa P. 2020 The failure of testing for cosmic opacity via the distance-duality relation. *Mon. Not. R. Astron. Soc.* **497**, 378–388. (doi:10.1093/mnras/staa1936)
64. Wright EL. 1982 Thermalization of starlight by elongated grains—could the microwave background have been produced by stars. *Astrophys. J.* **255**, 401–407. (doi:10.1086/159840)
65. Bond JR, Carr BJ, Hogan CJ. 1991 Cosmic backgrounds from primeval dust. *Astrophys. J.* **367**, 420–454. (doi:10.1086/169640)
66. Narlikar JV, Vishwakarma RG, Hajian A, Souradeep T, Burbidge G, Hoyle F. 2003 Inhomogeneities in the microwave background radiation interpreted within the framework of the quasi-steady state cosmology. *Astrophys. J.* **585**, 1–11. (doi:10.1086/345928)
67. Peacock JA. 1999 *Cosmological physics*, pp. 704. Cambridge, UK: Cambridge University Press.
68. Ryden B. 2016 *Introduction to cosmology*. Cambridge, UK: Cambridge University Press.
69. Mathis JS, Rumpl W, Nordsieck KH. 1977 The size distribution of interstellar grains. *Astrophys. J.* **217**, 425–433. (doi:10.1086/155591)
70. Jones AP, Tielens AGGM, Hollenbach DJ. 1996 Grain shattering in shocks: the interstellar grain size distribution. *Astrophys. J.* **469**, 740–764. (doi:10.1086/177823)
71. Draine BT, Fraisse AA. 2009 Polarized far-infrared and submillimeter emission from interstellar dust. *Astrophys. J.* **696**, 1–11. (doi:10.1088/0004-637X/696/1/1)
72. Davies JI, Alton P, Bianchi S, Trewhella M. 1998 The expulsion and retention of dust grains by galactic discs. *Mon. Not. R. Astron. Soc.* **300**, 1006–1014. (doi:10.1046/j.1365-8711.1998.01968.x)
73. Bianchi S, Ferrara A. 2005 Intergalactic medium metal enrichment through dust sputtering. *Mon. Not. R. Astron. Soc.* **358**, 379–396. (doi:10.1111/j.1365-2966.2005.08762.x)
74. Wright EL. 1987 Long-wavelength absorption by fractal dust grains. *Astrophys. J.* **320**, 818. (doi:10.1086/165597)
75. Flynn GJ. 1994 Interplanetary dust particles collected from the stratosphere: physical, chemical, and mineralogical properties and implications for their sources. *Planet. Space Sci.* **42**, 1151–1161. (doi:10.1016/0032-0633(94)90014-0)
76. Kocifaj M, Kapisinsky I, Kundracik F. 1999 Optical effects of irregular cosmic dust particle U2015 B10. *J. Quant. Spectrosc. Radiat. Transf.* **63**, 1–14. (doi:10.1016/S0022-4073(98)00130-7)
77. Kohout T *et al.* 2014 Density, porosity, mineralogy, and internal structure of cosmic dust and alteration of its properties during high-velocity atmospheric entry. *Meteorit. Planet. Sci.* **49**, 1157–1170. (doi:10.1111/maps.12325)

78. Weingartner JC, Draine BT. 2001 Dust grain-size distributions and extinction in the milky way, large magellanic cloud, and small magellanic cloud. *Astrophys. J.* **548**, 296–309. (doi:10.1086/318651)
79. Hauser MG, Dwek E. 2001 The cosmic infrared background: measurements and implications. *Annu. Rev. Astron. Astrophys.* **39**, 249–307. (doi:10.1146/annurev.astro.39.1.249)
80. Lagache G, Puget J-L, Dole H. 2005 Dusty infrared galaxies: sources of the cosmic infrared background. *Annu. Rev. Astron. Astrophys.* **43**, 727–768. (doi:10.1146/annurev.astro.43.072103.150606)
81. Cooray A. 2016 Extragalactic background light measurements and applications. *R. Soc. Open Sci.* **3**, 150555. (doi:10.1098/rsos.150555)
82. Madau P, Pozzetti L. 2000 Deep galaxy counts, extragalactic background light and the stellar baryon budget. *Mon. Not. R. Astron. Soc.* **312**, L9–L15. (doi:10.1046/j.1365-8711.2000.03268.x)
83. Kneiske TM, Bretz T, Mannheim K, Hartmann DH. 2004 Implications of cosmological gamma-ray absorption. *Astron. Astrophys.* **413**, 807–815. (doi:10.1051/0004-6361:20031542)
84. Dwek E, Krennrich F. 2005 Simultaneous constraints on the spectrum of the extragalactic background light and the intrinsic TeV spectra of Markarian 421, Markarian 501, and H1426 + 428. *Astrophys. J.* **618**, 657–674. (doi:10.1086/426010)
85. Primack JR, Domínguez A, Gilmore RC, Somerville RS. 2011 Extragalactic background light and gamma-ray attenuation. In *American Institute of Physics Conference Series*, vol. 1381 (eds FA Aharonian, W Hofmann, FM Rieger), pp. 72–83. New York, NY: AIP Publishing. (doi:10.1063/1.3635825)
86. Gilmore RC, Somerville RS, Primack JR, Domínguez A. 2012 Semi-analytic modelling of the extragalactic background light and consequences for extragalactic gamma-ray spectra. *Mon. Not. R. Astron. Soc.* **422**, 3189–3207. (doi:10.1111/j.1365-2966.2012.20841.x)
87. Bernstein RA, Freedman WL, Madore BF. 2002 The first detections of the extragalactic background light at 3000, 5500, and 8000 Å. I. Results. *Astrophys. J.* **571**, 56–84. (doi:10.1086/339422)
88. Bernstein RA, Freedman WL, Madore BF. 2002 The first detections of the extragalactic background light at 3000, 5500, and 8000 Å. II. Measurement of foreground zodiacal light. *Astrophys. J.* **571**, 85–106. (doi:10.1086/339423)
89. Bernstein RA, Freedman WL, Madore BF. 2002 The first detections of the extragalactic background light at 3000, 5500, and 8000 Å. III. Cosmological implications. *Astrophys. J.* **571**, 107–128. (doi:10.1086/339424)
90. Bernstein RA. 2007 The optical extragalactic background light: revisions and further comments. *Astrophys. J.* **666**, 663–673. (doi:10.1086/519824)
91. Schechter P. 1976 An analytic expression for the luminosity function for galaxies. *Astrophys. J.* **203**, 297. (doi:10.1086/154079)
92. Cross N *et al.* 2001 The 2dF galaxy redshift survey: the number and luminosity density of galaxies. *Mon. Not. R. Astron. Soc.* **324**, 825–841. (doi:10.1046/j.1365-8711.2001.04254.x)
93. Blanton MR *et al.* 2001 The luminosity function of galaxies in SDSS commissioning data. *Astron. J.* **121**, 2358–2380. (doi:10.1086/320405)
94. Blanton MR *et al.* 2003 The galaxy luminosity function and luminosity density at redshift $z = 0.1$. *Astrophys. J.* **592**, 819–838. (doi:10.1086/375776)
95. Brown WR, Geller MJ, Fabricant DG, Kurtz MJ. 2001 *V*- and *R*-band galaxy luminosity functions and low surface brightness galaxies in the century survey. *Astron. J.* **122**, 714–728. (doi:10.1086/321176)
96. Bahcall NA, Lubin LM, Dorman V. 1995 Where is the dark matter? *Astrophys. J.* **447**, L81. (doi:10.1086/309577)
97. Penton SV, Stocke JT, Shull JM. 2002 The local Lyα forest. III. Relationship between Lyα absorbers and galaxies, voids, and superclusters. *Astrophys. J.* **565**, 720–742. (doi:10.1086/324483)
98. Tejos N, Morris SL, Crighton NHM, Theuns T, Altay G, Finn CW. 2012 Large-scale structure in absorption: gas within and around galaxy voids. *Mon. Not. R. Astron. Soc.* **425**, 245–260. (doi:10.1111/j.1365-2966.2012.21448.x)
99. Tejos N *et al.* 2014 On the connection between the intergalactic medium and galaxies: the H_I—galaxy cross-correlation at $z \leq 1$. *Mon. Not. R. Astron. Soc.* **437**, 2017–2075. (doi:10.1093/mnras/stt1844)

100. Bielby R, Crighton NHM, Fumagalli M, Morris SL, Stott JP, Tejos N, Cantalupo S. 2017 Probing the intra-group medium of a $z = 0.28$ galaxy group. *Mon. Not. R. Astron. Soc.* **468**, 1373–1386. (doi:10.1093/mnras/stx528)
101. Wakker BP, Hernandez AK, French DM, Kim T-S, Oppenheimer BD, Savage BD. 2015 Nearby galaxy filaments and the Lyα forest: confronting simulations and the UV background with observations. *Astrophys. J.* **814**, 40. (doi:10.1088/0004-637X/814/1/40)
102. Nicastro F *et al.* 2018 Observations of the missing baryons in the warm–hot intergalactic medium. *Nature* **558**, 406–409. (doi:10.1038/s41586-018-0204-1)
103. Pessa I *et al.* 2018 A VLT/MUSE galaxy survey towards QSO Q1410: looking for a WHIM traced by BLAs in inter-cluster filaments. *Mon. Not. R. Astron. Soc.* **477**, 2991–3013. (doi:10.1093/mnras/sty723)
104. Ade PAR *et al.* Planck Collaboration. 2016 *Planck* 2015 results. XIII. Cosmological parameters. *Astron. Astrophys.* **594**, A13. (doi:10.1051/0004-6361/201525830)
105. Aghanim N *et al.* Planck Collaboration. 2018 Planck 2018 results. VI. Cosmological parameters. (https://arxiv.org/abs/1807.06209). (doi:10.1016/S0370-1573(98)00080-5).
106. Birkinshaw M. 1999 The Sunyaev–Zel'dovich effect. *Phys. Rep.* **310**, 97–195. (doi:10.1016/S0370-1573(98)00080-5)
107. Bonamente M, Joy MK, LaRoque SJ, Carlstrom JE, Reese ED, Dawson KS. 2006 Determination of the cosmic distance scale from Sunyaev-Zel'dovich effect and *Chandra* X-ray measurements of high-redshift galaxy clusters. *Astrophys. J.* **647**, 25–54. (doi:10.1086/505291)
108. Carlstrom JE, Holder GP, Reese ED. 2002 Cosmology with the Sunyaev-Zel'dovich effect. *Annu. Rev. Astron. Astrophys.* **40**, 643–680. (doi:10.1146/annurev.astro.40.060401.093803)
109. Suyu SH *et al.* 2013 Two accurate time-delay distances from strong lensing: implications for cosmology. *Astrophys. J.* **766**, 70. (doi:10.1088/0004-637X/766/2/70)
110. Bonvin V *et al.* 2017 H0LiCOW—V. New COSMOGRAIL time delays of HE 0435-1223: H_0 to 3.8 per cent precision from strong lensing in a flat ΛCDM model. *Mon. Not. R. Astron. Soc.* **465**, 4914–4930. (doi:10.1093/mnras/stw3006)
111. Vitale S, Chen H-Y. 2018 Measuring the Hubble constant with neutron star black hole mergers. *Phys. Rev. Lett.* **121**, 021303. (doi:10.1103/PhysRevLett.121.021303)
112. Howlett C, Davis TM. 2020 Standard siren speeds: improving velocities in gravitational-wave measurements of H_0. *Mon. Not. R. Astron. Soc.* **492**, 3803–3815. (doi:10.1093/mnras/staa049)
113. Abbott BP *et al.* 2017 A gravitational-wave standard siren measurement of the Hubble constant. *Nature* **551**, 85–88. (doi:10.1038/nature24471)
114. Jackson N. 2015 The Hubble constant. *Living Rev. Relativ.* **18**, 2. (doi:10.1007/lrr-2015-2)
115. Freedman WL *et al.* 2001 Final results from the *Hubble Space Telescope* key project to measure the Hubble constant. *Astrophys. J.* **553**, 47–72. (doi:10.1086/320638)
116. Riess AG, Macri L, Casertano S, Lampeitl H, Ferguson HC, Filippenko AV, Jha SW, Li W, Chornock R. 2011 A 3% solution: determination of the Hubble constant with the *Hubble Space Telescope* and wide field camera 3. *Astrophys. J.* **730**, 119. (doi:10.1088/0004-637X/730/2/119)
117. Riess AG *et al.* 2016 A 2.4% determination of the local value of the Hubble constant. *Astrophys. J.* **826**, 56. (doi:10.3847/0004-637X/826/1/56)
118. Riess AG *et al.* 2018 Milky Way Cepheid standards for measuring cosmic distances and application to *Gaia* DR2: implications for the Hubble constant. *Astrophys. J.* **861**, 126. (doi:10.3847/1538-4357/aac82e)
119. Freedman WL *et al.* 2019 The Carnegie-Chicago Hubble program. VIII. An independent determination of the Hubble constant based on the tip of the red giant branch. *Astrophys. J.* **882**, 34. (doi:10.3847/1538-4357/ab2f73)
120. Clarkson C, Cortês M, Bassett B. 2007 Dynamical dark energy or simply cosmic curvature? *J. Cosmol. Astropart. Phys.* **2007**, 011 (doi:10.1088/1475-7516/2007/08/011)
121. Li Z, Wang G-J, Liao K, Zhu Z-H. 2016 Model-independent estimations for the curvature from standard candles and clocks. *Astrophys. J.* **833**, 240. (doi:10.3847/1538-4357/833/2/240)
122. Wei J-J, Wu X-F. 2017 An improved method to measure the cosmic curvature. *Astrophys. J.* **838**, 160. (doi:10.3847/1538-4357/aa674b)
123. Yu H, Wang FY. 2016 New model-independent method to test the curvature of the universe. *Astrophys. J.* **828**, 85. (doi:10.3847/0004-637X/828/2/85)
124. Qi J-Z, Cao S, Pan Y, Li J. 2019 Cosmic opacity: cosmological-model-independent tests from gravitational waves and Type Ia supernova. *Phys. Dark Univ.* **26**, 100338. (doi:10.1016/j.dark.2019.100338)

125. Liao K. 2019 The cosmic distance duality relation with strong lensing and gravitational waves: an opacity-free test. *Astrophys. J.* **885**, 70. (doi:10.3847/1538-4357/ab4819)
126. Bond HE, Nelan EP, VandenBerg DA, Schaefer GH, Harmer D. 2013 HD 140283: a star in the solar neighborhood that formed shortly after the Big Bang. *Astrophys. J. Lett.* **765**, L12. (doi:10.1088/2041-8205/765/1/L12)
127. Venemans BP *et al.* 2017 Copious amounts of dust and gas in a $z = 7.5$ quasar host galaxy. *Astrophys. J.* **851**, L8. (doi:10.3847/2041-8213/aa943a)
128. Oesch PA *et al.* 2016 A remarkably luminous galaxy at $z = 11.1$ measured with *Hubble Space Telescope* grism spectroscopy. *Astrophys. J.* **819**, 129. (doi:10.3847/0004-637X/819/2/129)
129. Hashimoto T *et al.* 2018 The onset of star formation 250 million years after the Big Bang. *Nature* **557**, 392–395. (doi:10.1038/s41586-018-0117-z)
130. Hoag A *et al.* 2018 *HST* grism observations of a gravitationally lensed redshift 9.5 galaxy. *Astrophys. J.* **854**, 39. (doi:10.3847/1538-4357/aaa9c2)
131. Oesch PA, Bouwens RJ, Illingworth GD, Labbé I, Stefanon M. 2018 The dearth of $z \sim 10$ galaxies in all *HST* legacy fields—the rapid evolution of the galaxy population in the first 500 Myr. *Astrophys. J.* **855**, 105. (doi:10.3847/1538-4357/aab03f)
132. Salmon B *et al.* 2018 RELICS: a candidate $z \sim 10$ galaxy strongly lensed into a spatially resolved arc. *Astrophys. J.* **864**, L22. (doi:10.3847/2041-8213/aadc10)
133. Riess AG *et al.* 1998 Observational evidence from supernovae for an accelerating universe and a cosmological constant. *Astron. J.* **116**, 1009–1038. (doi:10.1086/300499)
134. Perlmutter S *et al.* 1999 Measurements of Ω and Λ from 42 high-redshift supernovae. *Astrophys. J.* **517**, 565–586. (doi:10.1086/307221)
135. Weinberg DH, Mortonson MJ, Eisenstein DJ, Hirata C, Riess AG, Rozo E. 2013 Observational probes of cosmic acceleration. *Phys. Rep.* **530**, 87–255. (doi:10.1016/j.physrep.2013.05.001)
136. Sakstein J, Jain B. 2017 Implications of the neutron star merger GW170817 for cosmological scalar-tensor theories. *Phys. Rev. Lett.* **119**, 251303. (doi:10.1103/PhysRevLett.119.251303)
137. Ezquiaga JM, Zumalacárregui M. 2017 Dark energy after GW170817: dead ends and the road ahead. *Phys. Rev. Lett.* **119**, 251304. (doi:10.1103/PhysRevLett.119.251304)
138. Vavryčuk V. 2017 Missing dust signature in the cosmic microwave background. *Mon. Not. R. Astron. Soc.* **470**, L44–L48. (doi:10.1093/mnrasl/slx069)
139. Vielva P, Martínez-González E, Barreiro RB, Sanz JL, Cayón L. 2004 Detection of non-Gaussianity in the *Wilkinson microwave anisotropy probe* first-year data using spherical wavelets. *Astrophys. J.* **609**, 22–34. (doi:10.1086/421007)
140. Cruz M, Martínez-González E, Vielva P, Cayón L. 2005 Detection of a non-Gaussian spot in WMAP. *Mon. Not. R. Astron. Soc.* **356**, 29–40. (doi:10.1111/j.1365-2966.2004.08419.x)
141. Ade PAR *et al.* Planck Collaboration. 2014 *Planck* 2013 results. XXIV. Constraints on primordial non-Gaussianity. *Astron. Astrophys.* **571**, A24. (doi:10.1051/0004-6361/201321554)
142. Lazarian A, Prunet S. 2002 Polarized microwave emission from dust. In *Astrophysical Polarized Backgrounds*, vol. 609 (eds S Cecchini, S Cortiglioni, R Sault, C Sbarra). American Institute of Physics Conference Series, pp. 32–43. New York, NY: AIP Publishing. (doi:10.1063/1.1471820)
143. Gold B *et al.* 2011 Seven-year *Wilkinson microwave anisotropy probe* (*WMAP*) observations: galactic foreground emission. *Astrophys. J. Suppl.* **192**, 15. (doi:10.1088/0067-0049/192/2/15)
144. Ichiki K. 2014 CMB foreground: a concise review. *Prog. Theor. Exp. Phys.* **2014**, 06B109. (doi:10.1093/ptep/ptu065)
145. Ade PAR *et al.* Planck Collaboration. 2015 *Planck* intermediate results. XIX. An overview of the polarized thermal emission from Galactic dust. *Astron. Astrophys.* **576**, A104. (doi:10.1051/0004-6361/201424082)
146. Aghanim N *et al.* Planck Collaboration. 2016 *Planck* intermediate results. *Astron. Astrophys.* **596**, A109. (doi:10.1051/0004-6361/201629022)
147. Kippenhahn R, Weigert A, Weiss A. 2012 *Stellar structure and evolution*. Astronomy and Astrophysics Library. Berlin, Heidelberg: Springer.
148. Zinnecker H, Yorke HW. 2007 Toward understanding massive star formation. *Annu. Rev. Astron. Astrophys.* **45**, 481–563. (doi:10.1146/annurev.astro.44.051905.092549)
149. Martin CL. 2005 Mapping large-scale gaseous outflows in ultraluminous galaxies with Keck II ESI spectra: variations in outflow velocity with galactic mass. *Astrophys. J.* **621**, 227–245. (doi:10.1086/427277)
150. Hopkins PF, Quataert E, Murray N. 2012 Stellar feedback in galaxies and the origin of galaxy-scale winds. *Mon. Not. R. Astron. Soc.* **421**, 3522–3537. (doi:10.1111/j.1365-2966.2012.20593.x)

151. Segers MC, Crain RA, Schaye J, Bower RG, Furlong M, Schaller M, Theuns T. 2016 Recycled stellar ejecta as fuel for star formation and implications for the origin of the galaxy mass–metallicity relation. *Mon. Not. R. Astron. Soc.* **456**, 1235–1258. (doi:10.1093/mnras/stv2562)
152. Anglés-Alcázar D, Faucher-Giguère C-A, Kereš D, Hopkins PF, Quataert E, Murray N. 2017 The cosmic baryon cycle and galaxy mass assembly in the FIRE simulations. *Mon. Not. R. Astron. Soc.* **470**, 4698–4719. (doi:10.1093/mnras/stx1517)
153. Muzahid S, Kacprzak GG, Churchill CW, Charlton JC, Nielsen NM, Mathes NL, Trujillo-Gomez S. 2015 An extreme metallicity, large-scale outflow from a star-forming galaxy at $z \sim 0.4$. *Astrophys. J.* **811**, 132 (doi:10.1088/0004-637X/811/2/132)
154. Hatch N. 2016 Galaxy formation through cosmic recycling. *Science* **354**, 1102–1103. (doi:10.1126/science.aah6255)
155. Muratov AL *et al.* 2017 Metal flows of the circumgalactic medium, and the metal budget in galactic haloes. *Mon. Not. R. Astron. Soc.* **468**, 4170–4188. (doi:10.1093/mnras/stx667)
156. Brennan R, Choi E, Somerville RS, Hirschmann M, Naab T, Ostriker JP. 2018 Momentum-driven winds from radiatively efficient black hole accretion and their impact on galaxies. *Astrophys. J.* **860**, 14. (doi:10.3847/1538-4357/aac2c4)
157. Rauch M. 1998 The Lyman alpha forest in the spectra of quasistellar objects. *Annu. Rev. Astron. Astrophys.* **36**, 267–316. (doi:10.1146/annurev.astro.36.1.267)
158. Pettini M. 2004 Cosmochemistry: the melting pot of the elements. In *Cosmochemistry. The melting pot of the elements* (eds C Esteban, R García López, A Herrero, F Sánchez), pp. 257–298. Cambridge, UK: Cambridge University Press. (doi:10.1071/AS12005)
159. Kroupa P. 2012 The dark matter crisis: falsification of the current standard model of cosmology. *Publ. Astron. Soc. Aust.* **29**, 395–433. (doi:10.1071/AS12005)
160. Kroupa P. 2015 Galaxies as simple dynamical systems: observational data disfavor dark matter and stochastic star formation. *Can. J. Phys.* **93**, 169–202. (doi:10.1139/cjp-2014-0179)
161. Buchert T, Coley AA, Kleinert H, Roukema BF, Wiltshire DL. 2016 Observational challenges for the standard FLRW model. *Int. J. Mod. Phys. D* **25**, 1630007. (doi:10.1142/S021827181630007X)
162. Bullock JS, Boylan-Kolchin M. 2017 Small-scale challenges to the ΛCDM paradigm. *Annu. Rev. Astron. Astrophys.* **55**, 343–387. (doi:10.1146/annurev-astro-091916-055313)
163. Einstein A. 1917 Sitzungsberichte der Königlich Preußischen Akademie der Wissenschaften. Berlin: Deutsche Akademie der Wissenschaften zu Berlin, p. 142.